FEBS Letters

FEBS PRESS science publishing by scientists

EDITOR'S CHOICE

Synaptic signalling in a network of dopamine neurons: what prevents proper intercellular crosstalk?

Yixi Chen[1,2], Tilo Kunath[1,2], Joanna Simpson[3], Natalie Homer[3] and Sergiy Sylantyev[4]

1 MRC Centre for Regenerative Medicine, Institute for Stem Cell Research, University of Edinburgh, Edinburgh, UK
2 UK Centre for Mammalian Synthetic Biology, University of Edinburgh, Edinburgh, UK
3 Mass Spectrometry Core, Edinburgh Clinical Research Facility, Queen's Medical Research Institute, University of Edinburgh, Edinburgh, UK
4 Rowett Institute, University of Aberdeen, Aberdeen, UK

Correspondence
S. Sylantyev, Rowett Institute, University of Aberdeen, Ashgrove Road West, Aberdeen AB25 2ZD, UK
Tel: +441224437366
E-mail: s.sylantyev@abdn.ac.uk

(Received 14 July 2020, revised 6 August 2020, accepted 7 August 2020, available online 30 August 2020)

doi:10.1002/1873-3468.13910

Edited by Maurice Montal

Human embryonic stem cell (hESC)-derived midbrain dopamine (DA) neurons stand out as a cell source for transplantation with their sustainability and consistency superior to the formerly used fetal tissues. However, multiple studies of DA neurons in culture failed to register action potential (AP) generation upon synaptic input. To test whether this is due to deficiency of NMDA receptor (NMDAR) coagonists released from astroglia, we studied the functional properties of neural receptors in hESC-derived DA neuronal cultures. We find that, apart from an insufficient amount of coagonists, lack of interneuronal crosstalk is caused by hypofunction of synaptic NMDARs due to their direct inhibition by synaptically released DA. This inhibitory tone is independent of DA receptors and affects the NMDAR coagonist binding site.

Keywords: dopamine; dopamine neurons; human embryonic stem cells; NMDA receptor; synaptic signalling

Morphological studies provide the most detailed description of human neural development, outlining a multicomponent process of neurogenesis, where early neuroepithelial cells form neural networks and major CNS elements [1]. These studies, however, do not answer the question of how a naïve stem cell becomes a functionally mature neuron, since they do not monitor electrophysiological properties, which are critical for neuronal function, at the cellular and molecular level. In contrast, observations of human embryonic stem cells (hESCs), capable of differentiation into the majority of known cell types [2,3], allow systematic evaluation of a neuron's functional development under highly reproducible conditions, since hESCs can be patterned into region- and function-specific cells [4,5], in particular into dopamine (DA) neurons [6,7]. Of note is that the early stages of hESC-derived neuronal differentiation correspond to the early developmental stages of corresponding neuron types in the prenatal and neonatal brain [8]. In accordance with these observations, hESC-derived DA neurons in culture display slow functional development when compared to other neural cell types [7], as was revealed by the slowly developing electrophysiological properties of DA neurons in the native midbrain [9].

Abbreviations
AMPARs, AMPA receptors; AP, action potential; AUC, area under the response curve; BDNF, brain-derived neurotrophic factor; CNS, central nervous system; D2R, dopamine receptors of type 2; DA, dopamine; DIV, days *in vitro*; D-Ser, D-serine; EPSCs, excitatory postsynaptic currents; EPSPs, evoked postsynaptic potentials; $GABA_AR$, GABA-A receptor; Gly, glycine; hESC, Human embryonic stem cell; hiPS, human-induced pluripotent stem cell; IPSCs, inhibitory postsynaptic currents; NDM, neural differentiation medium; NIM, neural induction medium; NMDARs, NMDA receptors; NPM, neural patterning medium; OTF, open-time fraction; PD, Parkinson's disease; sEPSCs, spontaneous EPSCs; sPSCs, spontaneous postsynaptic currents; TH, tyrosine hydroxylase.

FEBS Letters **594** (2020) 3272–3292 © 2020 The Authors. *FEBS Letters* published by John Wiley & Sons Ltd on behalf of Federation of European Biochemical Societies
This is an open access article under the terms of the Creative Commons Attribution License, which permits use, distribution and reproduction in any medium, provided the original work is properly cited.

Parkinson's disease (PD) is a neurodegenerative disorder, which affects ~ 1% of the human population over 60 years old. Currently, cell replacement therapy provides a promising approach for PD treatment, as its physiological restoration of the dopaminergic system alleviates motor symptoms and can result in a reduced dependency on levodopa medication [10]. Such rebuilding of the dopaminergic network is not possible by popular treatments such as deep brain stimulation [11]. Fetal midbrain tissues were formerly used for such cell replacement therapy with variable results [12–14], but are now being replaced by more consistent and sustainable cell sources such as midbrain DA progenitors derived from hESCs or human-induced pluripotent stem cells (hiPSCs). The hESC/hiPSC-derived midbrain DA progenitors matured into midbrain DA neurons *in vivo* after transplantation and were comparably potent and efficient in rescuing animal PD models as fetal midbrain tissues [15,16]. The first patients with hiPSC-derived grafts have been transplanted [17] with more clinical trials in preparation [18,19]. The key requirement for transplantable cells is indeed the ability to interconnect with host neural tissue and thus establish the controlled DA release needed for restoration of normal CNS functioning.

Electrophysiological characterization of hESC-derived neurons is a common element performed in the course of development of a vast majority of differentiation protocols [6,20,21]. Electrophysiological studies of hESC-derived neurons have revealed a wide range of molecular actors supporting interneuronal signalling: first, receptors of main excitatory and inhibitory neurotransmitters: AMPA receptors (AMPARs) [22–24], NMDA receptors (NMDARs) [23,25], $GABA_A$ receptors ($GABA_A$Rs) [22,26], glycine receptors (GlyRs) [26], acetylcholine receptors [22], etc; and second, functional voltage-gated sodium, potassium and calcium channels [25,27,28]. This was supported by the observation of functional $GABA_B$ receptors in mouse ESCs [29], thus suggesting the full set of molecular elements needed for neural signalling to be present. Next, hESC-derived neurons were repeatedly shown to generate single [30,31] and/or multiple [32,33] action potentials (APs), both upon current injection and spontaneously [34]. In addition, spontaneous and evoked inhibitory postsynaptic currents (IPSCs) and excitatory postsynaptic currents (EPSCs) were found in neural networks composed from hESC-derived neurons, thus revealing the presence of fully functional synapses [35].

Being a subset of hESC-derived neurons, DA neurons possess the main subtypes of functional inhibitory ($GABA_A$Rs, GlyRs) [36,37] and excitatory (AMPARs, NMDARs) [27] receptors, whereas gaining of full receptors' functionality accompanies the cell differentiation and maturation [27]. Together with observations of GABA/DA corelease [38] and glutamate/DA corelease [39,40], this suggests normal synaptic signalling to be present between pairs of DA neurons. Nevertheless, to the best of our knowledge, to date there are no data confirming interneuronal synaptic crosstalk evoking APs firing in cultured hESC-derived DA neural networks. This is in line with our pilot experiments, where we failed to generate network-delivered AP (s) with the same experimental protocol [41] as had successfully been used previously to evoke I/EPSCs by extracellular stimulation in non-DA hESC-derived neural cultures [35] (Fig. 2C).

Our pilot results thus reproduce an earlier study, where hESC-derived DA neurons did generate APs upon current injection, but not in response to extracellular stimulation [42]. Notably, after 49 days *in vitro* (DIV) hESC-derived non-DA neurons were shown to generate evoked postsynaptic potentials (EPSPs) exclusively with AMPARs, but without any detectable NMDAR input. This was interpreted as a sign of immature synapses [43].

Hence, in this study we set out to clarify the limiting factor(s) preventing interneuronal crosstalk and generation of APs in response to synaptic input in a network of hESC-derived DA neurons. Taking into account data on slow maturation of DA neurons [7,9] and possible low NMDAR functionality in hESC-derived neural cells [43], we decided to investigate these factors foremost.

Materials and methods

Generation of DA neurons

Dopamine neurons were differentiated from hESCs (RC17, passage 27) as previously described [44]. Briefly, hESCs were self-renewed in StemMACS iPS-Brew XF (Miltenyi Biotec, Bisley, UK) on Laminin-521 (Biolamina, Stockholm, Sweden) and mycoplasma tested with negative result. Whole-genome single nucleotide polymorphism array analysis did not reveal any copy-number variations other than what was previously reported [45]. On differentiation day 0, hESCs were seeded at 40 000 cells per cm^2 onto Laminin-111 (Biolamina)-coated 24-well plates (Corning, Corning, NY, USA) according to adaption from a published floor plate protocol for midbrain DA differentiation [46].

From day 0 to 4, cells were differentiated in neural induction medium (NIM), which is 50% Dulbecco's Modified Eagle's medium/F12 (Thermo Fisher Scientific, Waltem, MA, USA) + 50% Neurobasal media (Thermo Fisher

Scientific) + B27 supplement (without vitamin A, 1 : 50; Thermo Fisher Scientific) + N2 supplement (1 : 100; Thermo Fisher Scientific) + L-glutamine (2 mM; Thermo Fisher Scientific). From day 4 to 11, cells were differentiated in neural patterning medium (NPM), the component of which was similar to NIM apart from the concentration of B27 and N2 supplement that was half of NIM. From day 11, cells were differentiated in neural differentiation medium (NDM), which was Neurobasal Media + B27 supplement (1 : 50) + L-glutamine (2 mM).

From day 0 to 9, SB431542 (SB, 10 μM; Millipore, Burlington, MA, USA), LDN-193189 (LDN, 100 ng·mL^{-1}; Miltenyi Biotec), Shh-C24II (SHH, 600 ng·mL^{-1}; R&D Systems) and CHIR99021 (CHIR, 1.0 μM; Miltenyi Biotec) were added in NIM or NPM and medium was changed on day 2, 4 and 7. From day 9 to 11, FGF8b (100 ng·mL^{-1}; R&D Systems, Minneapolis, MN, USA) and heparin (1 μg·mL^{-1}; Sigma, Dorset, UK) were added to NPM. On day 11, cells were lifted with Accutase (Sigma) and replated onto Laminin-111-coated 24-well plates at 800 000 cells per cm^2. From day 11 to 16, FGF8b, heparin, ascorbic acid (AA, 0.2 mM; Sigma), brain-derived neurotrophic factor (BDNF, 20 ng·mL^{-1}; Peprotech, Neuilly-Sur-Seine, France) and glial cell line-derived neurotrophic factor (GDNF, 10 ng·mL^{-1}; Peprotech) were added to NDM. Cells were fed on day 14 and lifted with Accutase on day 16 followed by replating onto Laminin-111-coated 24-well plates at 800 000 cells per cm^2. From day 16, cells were fed every 2–3 days with NDM supplemented with BDNF, GDNF, AA, dibutyryl cyclic AMP 0.5 mM, (Sigma) and DAPT (1 μM; Tocris, Bristol, UK). On 23 DIV, cells were lifted with Accutase, replated onto polyornithine (0.0015%; Sigma) + Laminin-111-coated plates at 15 000 or 25 000 cells per cm^2 on coverslips (VWR) for electrophysiology, at 25 000 cells per cm^2 on 8-well glass bottom plates (Ibidi) for immunostaining, or at 80 000 cells per cm^2 on 24-well plates for HPLC. After day 23 replating, feeding frequency was reduced to weekly with half media change. From day 45, DAPT was omitted from the feeding medium. A step-by-step version of this protocol is available at: https://doi.org/10.17504/protocols.io.bddpi25n.

Immunostaining and image analysis

Cells were fixed with 4% PFA and blocked with 2% donkey serum (Sigma) or 2% goat serum (Sigma) in PBS-T [0.1% Triton X-100 (Fisher) in PBS (Thermo Fisher Scientific)]. Primary antibodies used are LMX1A (1 : 1000; Millipore), FOXA2 (1 : 100; Santa Cruz, Dallas, TX, USA), tyrosine hydroxylase (TH) (1 : 1000; Millipore), β-III tubulin (1 : 1000; Abcam, Cambridge, UK), synapsin (1 : 1000; Millipore), PSD95 (1 : 250; Biolegend, San Diego, CA, USA), PSD95 (1 : 1000; Thermo Fisher Scientific), NMDAR2A/B (1 : 200; Merck, Darmstadt, Germany), $GABA_AR\alpha1$ (1 : 1000; Abcam) and D2DR (1 : 250; Santa Cruz). Two PSD95 antibodies of different isotypes were used in order to enable the costaining with other markers, which have the same isotype with one of the PSD95 antibodies. Secondary antibodies including donkey anti-rabbit Alexa Fluor 488, donkey anti-goat Alexa Fluor 555, donkey anti-mouse Alexa Fluor 647, goat anti-mouse IgG2a Alexa Fluor 488, goat anti-mouse IgG1 Alexa Fluor 555, goat anti-rabbit IgG Alexa Fluor 555 and goat anti-mouse IgG2b Alexa Fluor 647 were purchased from Thermo Fisher Scientific and used at 1 : 1000. LMX1A/FOXA2 staining images was acquired with 10× on IX151 (Olympus, Tokyo, Japan). Tyrosine hydroxylase/β-III tubulin staining images were acquired with 20× on Eclipse Ti-E (Nikon, Tokyo, Japan).

Synaptic staining images were acquired with 60x oil on Eclipse Ti-E as z-stacks covering a range of 2.4 μm (25 slices at a step of 0.1 μm). The stack images were deconvoluted with HUYGENS (version 19.04; Scientific Volume Imaging BV, Hilversum, Netherlands), split into three channels that were subsequently thresholded with IMAGEJ (https://imagej.net). The thresholded images were input to MATLAB, where the script (credited to M. Colom-Cadena and T. Spires-Jones, University of Edinburgh) excluded the synaptic particles that were not overlapping with β-III tubulin as noise. Colocalization or overlapping of the remaining particles was analysed in 3D. Colocalization of synapsin and PSD95 particles was defined as < 1 μm apart with a particle of the costained marker. For each marker, the MATLAB script outputs the total number of particles and the number of particles colocalized or overlapped with the costained marker, based on which the percentage of colocalization + overlapping was calculated.

CORIN flow cytometry

On day 16, the cells were lifted with Accutase and washed with NDM. Cells were then centrifuged at 800 ***g*** for 2 min and resuspended with flow cytometry buffer, which was DPBS (without Mg^{2+} and Ca^{2+}; Sigma) supplemented with 2% FBS (Thermo Fisher Scientific). The resuspended cells were then split into 3 tubes, one unstained, one stained with rat anti-CORIN antibody (R&D Systems, 1 : 500) and one stained with isotype control (R&D Systems, 1 : 500) for 15 min on ice. The stained cells were washed with flow cytometry buffer and incubated with donkey anti-rat IgG Alexa Fluor 488 (Thermo Fisher Scientific) for 15 min on ice. The stained cells were then washed with flow cytometry buffer and analysed on BD FACSCalibur (BD Biosciences, Franklin Lakes, NJ, USA). The data were processed and plotted with FLOWJO (version 10.0.7; BD, Franklin Lakes, NJ, USA).

Dopamine UPLC-MS/MS analysis

Conditioned media were collected on 105 DIV after a full media change on 101 DIV. The samples were frozen on dry

ice immediately for transportation, and subsequently thawed and analysed on the same day at the Mass Spectrometry Core, Edinburgh Clinical Research Facility. DA was extracted from cell media by solid-phase extraction using Strata Strong Cation Exchange cartridges (55 μm, 100 mg·mL^{-1}; Phenomenex, Macclesfield, UK) and derivatized with propionic anhydride prior to LC-MS/MS. The method of Zhang *et al*. [47] was adapted and applied to cell media analysis. All samples were enriched with 1 ng dopamine-1,1,2,4-(dopamine-D4; Cerilliant, Round Rock, TX, USA) as internal standard and diluted with 0.1 M hydrochloric acid (400 μL). Cartridges were conditioned with 0.1 M HCl (400 μL), followed by methanol (400 μL). The sample (100 μL) was diluted with 0.1 M HCl (1 : 1), then loaded onto the cartridge, and washed with methanol (400 μL) and 0.1 M HCl (400 μL). The sample was slowly eluted over 5 min by addition of acetonitrile : propionic anhydride (90 : 10 v/v) with 2% pyridine (1 mL), followed by a second elution with acetonitrile (400 μL). The combined eluate was collected, capped and heated at 60 °C for 20 min to form a propionate derivative of DA. The solution was reduced to dryness under nitrogen at 40 °C and reconstituted in 100 μL of water:acetonitrile (90 : 10, v/v). A calibration standard curve of DA (0.025–10 ng) was prepared alongside the samples for quantitative analysis of DA in the samples.

Chromatographic separation was achieved on a Waters Acquity Classic UPLC System with an Acquity UPLC BEH C18 column (50 × 2.1 mm; 1.7 μm; Waters, Wilmslow, UK) protected by an Acquity in-line filter (Waters) and operated at 45 °C. The mobile phase consisted of 0.1% formic acid in water (A) and 0.1% formic acid in acetonitrile (B) at a flow rate of 0.5 mL·min^{-1}. Gradient elution was achieved with a total run time of 7.5 min from 15% to 85% B.

Dopamine was detected on a QTrap 5500 triple quadrupole mass spectrometer (Sciex, Warrington, UK) operated in positive ion electrospray mode (5.5 kV, 500 °C, ion source gas 1 at 60 psig and gas 2 at 40 psig). In multiple reaction mode, transitions monitored were *m/z* 322.0→136.9 and *m/z* 326.0→140.9 for DA and DA-D4, respectively, and peaks were eluted at 2.3 min. The peak area ratio of DA/ DA-D4 was used to calculate the amount of DA in the sample by linear regression analysis of a calibration curve (0.025–10 ng). Scoring of LC-MS data was performed by investigators unaware of the type of samples (control or preconditioned).

After sample collection for conditioned media, the cultures were fixed with 4% PFA and stained for TH, β-III tubulin and DAPI. For each 24 well, a 14-mm^2 area was imaged as a representative region at 10× with tiling on Ti-E. Number of cells were obtained by particle analysis of the DAPI channel and analysed for their positivity of TH and β-III tubulin. Based on the number of TH/β-III tubulin double-positive cells of the representative image, the total number of TH/β-III tubulin double-positive cells in each well was estimated as used for normalization of the level of DA detected by UPLC-MS/MS.

Electrophysiology

Visualized patch-clamp recordings from cultured neurons were performed using an infrared differential interference contrast imaging system. The perfusion solution contained the following (in mM): 119 NaCl, 2.5 KCl, 1.3 Na_2SO_4, 2.5 $CaCl_2$, 26.2 $NaHCO_3$ and 1 NaH_2PO_4, 22 glucose, and was continuously gassed with 95% O_2 and 5% CO_2, pH 7.35; 290–298 mOsm. The intracellular pipette solution for voltage-clamp experiments contained the following (in mM): 120.5 CsCl, 10 KOH-HEPES, 2 EGTA, 8 NaCl, 5 QX-314 Br^- salt, 2 Na-ATP and 0.3 Na-GTP. For current-clamp recordings, intracellular pipette solution contained the following (in mM): 126 K-gluconate, 4 NaCl, 5 HEPES, 15 glucose, 1 $K_2SO_4 \cdot 7H_2O$, 2 BAPTA and 3 Na-ATP. pH was adjusted to 7.2 and osmolarity adjusted to 295 mOsm. To isolate response of NMDARs, we added to perfusion solution 50 μM picrotoxin, 20 μM NBQX, 1 μM strychnine, 1 μM CGP-55845 and 100 μM MCPG, with no Mg^{2+} in perfusion solution. To isolate response of $GABA_A$Rs, we added 50 μM APV, 20 μM NBQX, 1 μM strychnine, 1 μM CGP-55845 and 100 μM MCPG. To isolate response of GlyRs, we added 50 μM picrotoxin, 20 μM NBQX, 50 μM APV, 1 μM CGP-55845 and 100 μM MCPG. To isolate response of AMPARs, we added 50 μM picrotoxin, 50 μM APV, 1 μM strychnine, 1 μM CGP-55845 and 100 μM MCPG.

Whole-cell recordings

Whole-cell recordings in current-clamp and voltage-clamp mode were performed at 32–34 °C; the patch pipette resistance was 3–7 MΩ depending on particular experimental conditions. Series resistance was monitored throughout experiments using a + 5 mV step command, and cells with very high series resistance (above 25 MΩ) or unstable holding current were rejected.

Outside-out and nucleated patch recordings

Outside-out patches and cell membrane bags containing intact nucleus and cytoplasm (nucleated patches) were pulled from cultured neurons, and recordings were performed in voltage-clamp mode (V_{hold} −60 or −70 mV, as indicated). Solution exchange experiments were performed as described in our earlier published protocol [48]. Briefly, we used a θ-glass application pipette with ~ 200 μm tip diameter attached to the micromanipulator. The position of the pipette was controlled by piezoelectric element (the speed of switch was 50–100 μs). One pipette channel was filled with the bath artificial cerebrospinal fluid solution;

another channel was loaded with neuroreceptors' ligands. Pressure was regulated by a PDES-02DX pneumatic microejector (npi) using compressed nitrogen separately in each of two channels.

We have chosen nucleated patches rather than outside-out patches due to the following considerations. Since nucleated patch preserves a part of intracellular milieu, this allows persistence of modulatory signalling from cytoplasmic actors, and therefore more physiological receptor response. However, in experiment on direct NMDAR block by DA we used outside-out rather than nucleated patches: since DAR-initiated inhibition of NMDARs requires involvement of cytoplasmic signalling cascades [49–51], this preparation makes sure that all cytoplasmic structures are destroyed.

Acquisition and analysis

Recordings were obtained using a MultiClamp 700B Amplifier (Molecular Devices, San Jose, CA, USA), filtered at 4–8 kHz, digitized at 10 kHz and stored on a PC. PCLAMP/CLAMPFIT 10× software (Molecular Devices) was used for data storage and offline analysis. Activation of neuroreceptors at outside-out and nucleated patches evoked macroscopic responses, where 'peak response' was obtained as a difference between baseline (average for 50 ms before application of NMDAR ligands) and maximum evoked current. For automatic detection of spontaneous postsynaptic currents (sPSCs), we used a Clampfit 10 built-in event detection algorithm with a detection template generated by averaging of 10–15 events with amplitude higher than doubled amplitude of peak-to-peak noise in given recording. To quantify charge transfer by EPSP events and changes in cell membrane capacitance due to neurotransmitter vesicle release, we used area under the response curve (AUC). This was obtained as Σ (a_n-a_c), where a_n is a current (or capacitance) value at a given time point after stimulation, and a_c is a baseline average for 100 ms before stimulation.

The open-time fraction (OTF) of single NMDAR channels was calculated as t_f/t_o, where t_f is a full time of observation, and t_o is a time in an open state. t_o was counted using a detection threshold of 1.5 pA more negative than mean baseline and a minimum opening time of 0.2 ms.

It was virtually impossible to determine accurately the number of channels in a membrane patch; however, in our preparation the vast majority of channel openings were single-level events. In a case where there were multiple levels of channel openings, only level with highest conductance was analysed. This prevented us from overestimation of opening frequency increase, since in multichannel patch, increased opening frequency would be accompanied by increase in proportion of multilevel events. Values for the average open time of single channel were obtained with threshold-detection algorithm of CLAMPFIT 10× software.

To fit the concentration–response curve of NMDA antagonists' effect on NMDAR OTF, we used the Hill equation:

$$\mathrm{OTF} = \frac{\mathrm{C_l^n}}{\mathrm{IC_{50}} + \mathrm{C_l^n}} \quad (1)$$

where C_l is concentration of a given ligand, IC_{50} is the concentration of a ligand generating half-maximum effect, and n is Hill's coefficient.

For numerical fitting of decay profiles of phasic responses recorded from NPs, we applied a generalized biexponential fitting approach:

$$\Delta I = -a_1 e^{-t/\tau_1} - a_2 e^{-t/\tau_2} \quad (2)$$

In (Eq. 2), ΔI is a difference between current recorded at baseline and at time t, e is Euler's constant, a is the fitting constant, and τ is the decay time constant. To quantify changes in response kinetics under different experimental conditions (application of pharmacological agents and/or changes of holding voltage), we used a 'fast decay component-to-slow decay component' ratio of fitting constants (a).

To test whether the effect of simultaneous application of DA and memantine at NMDARs is independent or not (i.e. whether these two drugs compete for the same binding site), we compared the standard error of sum of their independent effects (SE_{sum}) with standard error of the effect triggered by their joint application. SE_{sum} of effects x and y when the number of samples $n_x = n_y = n$ can be obtained as

$$\mathrm{SE_{sum}} = \frac{1}{\sqrt{n}}\sqrt{s_x^2 + s_y^2 + 2s_{xy}^2} \quad (3)$$

In (Eq. 3), s_x is a standard deviation of effect x; s_y is a standard deviation of effect y; s_{xy}^2 is a covariance of x, y. If factors x and y are independent, $s_{xy}^2 = 0$, and

$$\mathrm{SE_{sum}} = \frac{1}{\sqrt{n}}\sqrt{s_x^2 + s_y^2} \quad (4)$$

Strychnine, tetrabenazine (TBZ), memantine, GGP-55845, NBQX, DNQX, APV, picrotoxin, MCPG, QX-314 bromide, NMDA, glycine, (S)-sulpiride, felbamate, PMPA and SCH-23390 were purchased from Tocris Bioscience [52]. All other chemicals were purchased form Sigma-Aldrich, unless otherwise indicated. All data are given as mean ± standard error of mean. Statistical comparisons were made with Student's unpaired t-test, unless different is indicated in the text; P-value of ≤ 0.05 was taken as a threshold of significance.

Results

As a preliminary control, we assessed the quality of the midbrain DA differentiation of hESCs during both

progenitor stage and neuronal stage. On day 11, the cells were highly positive for LMX1A and FOXA2, suggesting their identity as midbrain DA progenitors (Fig. 1A) [46,53]. On day 16, flow cytometry of floor plate marker CORIN indicated the midbrain DA progenitors were of floor plate identity (Fig. 1B) [54]. On day 44, the midbrain DA culture was highly positive for DA marker TH (Fig. 1C) and expressed a high level of DA neuronal markers NURR1, SOX6, VMAT2 and DAT [44]. The high purity of TH-positive neurons was retained in further differentiation to day 77 (Fig. 1C).

In the first stage of our study, we performed characterization of electrophysiological properties of hESC-derived DA neurons. We tested, whether they carry functional ionotropic excitatory and inhibitory receptors of two main types: glutamate-sensitive (AMPARs, NMDARs) and GABA-sensitive ($GABA_A$Rs). To do this, we applied receptor-specific ligands at nucleated membrane patches. Application of 100 μM AMPA, 100 μM GABA and 100 μM NMDA + 100 μM Gly triggered transmembrane currents, then suppressed by specific antagonists of corresponding receptors: NBQX (20 μM), PTX (50 μM) and APV (50 μM), respectively (Fig. 2A).

In the second stage, we tested whether DA neurons can generate APs. Indeed, in response to current injection we observed APs, which were suppressed by 1 μM TTX, demonstrating the presence of voltage-gated sodium channels and their decisive role in AP generation (Fig. 2B).

Therefore, we next examined whether cultured DA neurons can generate APs in response to field stimulation, that is, whether they form a functional neural network with working synapses (Fig. 2C). To do this, we delivered a series of five field stimuli with 50-ms intervals. We tried to generate APs with this stimulation pattern in 21 cells (12 at 66 DIV, 9 at 100 DIV), which displayed APs in response to current injection, but all our attempts were fruitless. However, 50 μM

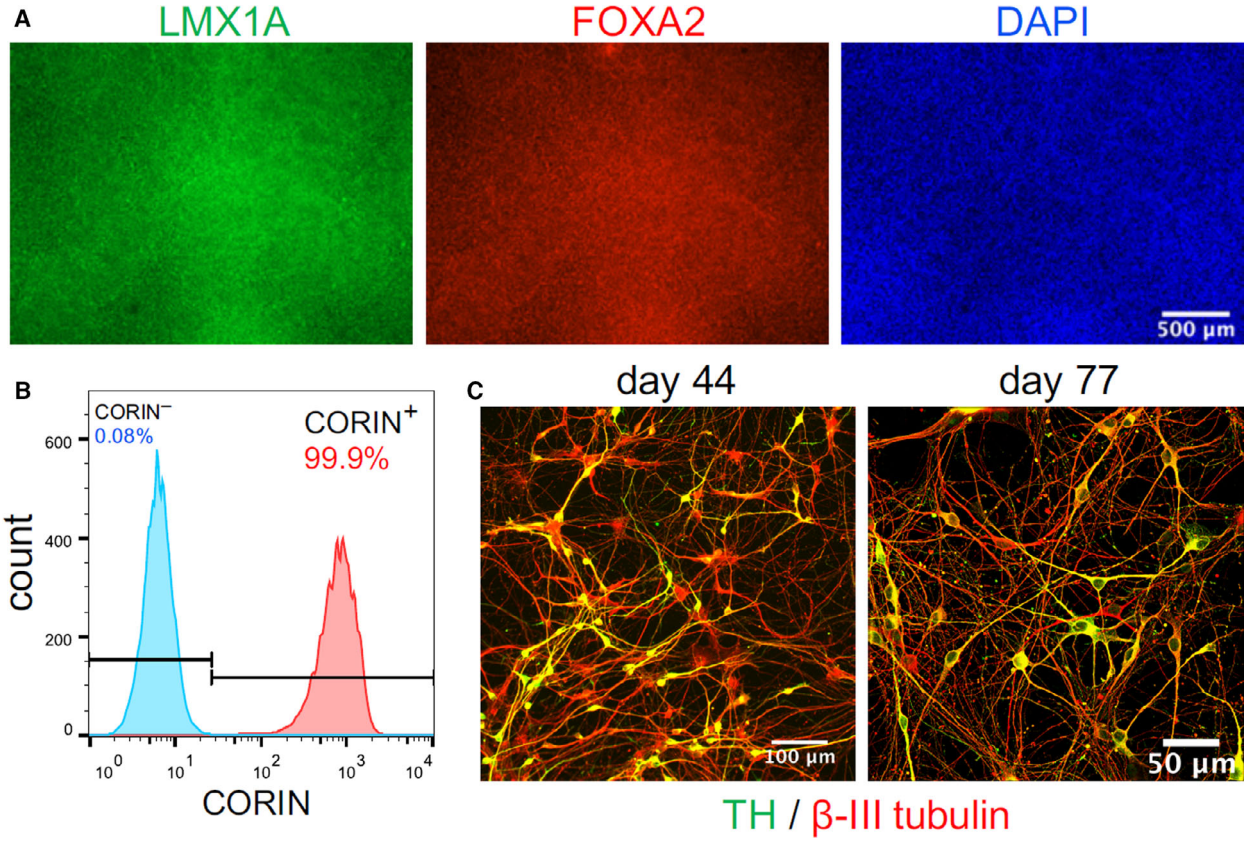

Fig. 1. Quality control of midbrain DA neuron differentiation. (A) Day 11 coimmunostaining of LMX1A and FOXA2 suggested a homogeneous population of midbrain DA progenitors. (B) Day 16 flow cytometry of CORIN indicated the vast majority of midbrain DA progenitors were of floor plate identity. (C) Typical day 44 and 77 coimmunostaining of DA marker TH and pan-neuronal marker β-III tubulin in mDA cultures plated at 25 000 cells per cm^2 on 8-well glass bottom plates.

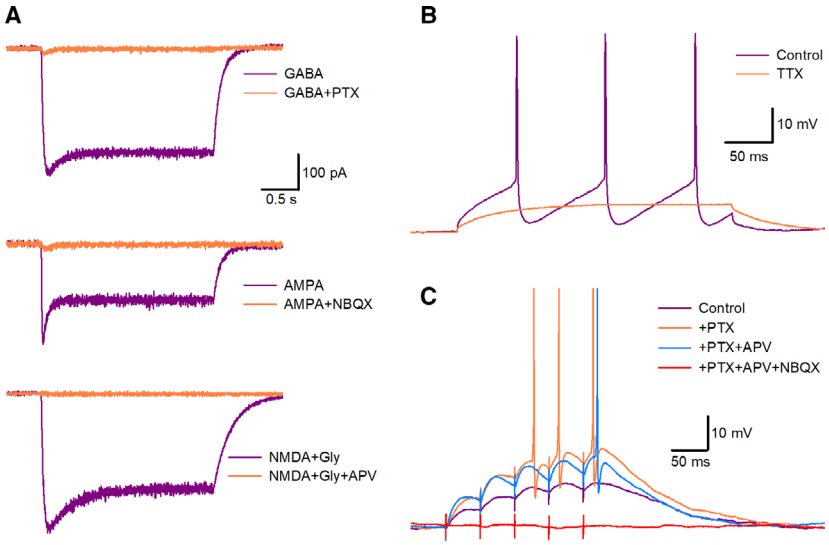

Fig. 2. NMDARs, despite being abundant at cell membrane, play a minor role in EPSP and AP generation. (A) Cultured DA neurons carry fully functional excitatory and inhibitory ionotropic receptors at their surface. Application of corresponding receptor agonist(s): 100 μM GABA, 100 μM AMPA, 100 μM NMDA + 100 μM glycine at nucleated membrane patches triggers current flow through $GABA_A$Rs, AMPARs and NMDARs, respectively. Further action of selective antagonists (50 μM PTX, 20 μM NBQX, 50 μM APV) confirms generation of observed transmembrane current exclusively by correspondent receptor. Scale bars in A apply to all traces. (B) APs triggered by step current injection. 1 μM TTX fully suppresses APs, confirming involvement of voltage-gated sodium channels. (C) EPSP generation by field stimulation. No APs were obtained under control conditions, whereas block of $GABA_A$Rs with 50 μM PTX triggered AP generation. Subsequent application of 50 μM APV demonstrates nonsignificant input of NMDARs into EPSP and AP generation machinery (see text for details and statistical data). In contrast, 20 μM NBQX, being added to perfusion solution, reveals a major input of AMPARs into EPSP formation.

PTX added to the perfusion solution triggered AP firing in 8 of 21 cells (4/12 at 66 DIV, 4/9 at 100 DIV). The 50 μM APV, added after PTX, did not generate a significant difference in a number of the APs per stimulation train: 2.375 ± 0.183 for PTX vs. 1.75 ± 0.164 for PTX + APV, $P = 0.095$, $n = 8$, Student's paired *t*-test. In contrast, 20 μM NBQX, added after APV, fully suppressed EPSPs in all 21 cells tested.

These initial results suggest that normal synaptic signalling in a cultured network of hESC-derived DA neurons is precluded due to the weak NMDAR function. Hence, we set out to clarify the factors determining such a poor NMDAR signalling. To find out whether this is due to under-differentiation of stem cells into neurons, we repeated all the experiments on 66 DIV and 100 DIV cultures. However, the only experimental readout with a significant difference between 66 DIV and 100 DIV was a frequency of $GABA_A$R-mediated spontaneous EPSCs (sEPSCs) under elevated Ca^{2+} concentration (Fig. 4).

Hence, as a first step, we tested whether DA neurons possess functional synapses. To do this, we performed immunostaining for PSD-95 (scaffolding element of postsynaptic density) and synapsin (presynaptic protein implicated into vesicle release of neurotransmitters) on 66 DIV. Close proximity of PSD-95 and synapsin staining foci should mark functional synapses. Indeed, in our experiments we found that $27.73 \pm 2.23\%$ of PSD-95 foci are placed within 1 μM distance from synapsin, and $23.89 \pm 3.89\%$ of synapsin foci are placed within 1 μM distance from PSD-95 (Fig. 3A, $n = 6$ fields from two cultures). Average numbers of 7.14 ± 0.89 PSD-95 particles were in close proximity with synapsin and 7.07 ± 0.88 synapsin particles were in close proximity with PSD-95 per 10 μm^3 in our preparation suggest numerous functional synapses within a neural network.

Next, we tested whether cultured neurons have functional presynaptic neurotransmitter release machinery. To do this, we recorded changes in a whole-cell membrane capacitance (C_m) in response to a field stimulation train of five stimuli with 50-ms intervals (Fig. 3B). To quantify the input of the Ca^{2+}-dependent mechanism of vesicle release, we repeated the experiment under normal (2 mM) and elevated (5 mM) Ca^{2+} concentration, and then calculated the normal/elevated ratio of AUC. The stimulation train triggered a clear transitional increase in C_m, whereas elevation of extracellular Ca^{2+} induced a significant increase in AUC (Fig. 3B). The control vs. elevated Ca^{2+} ratio was

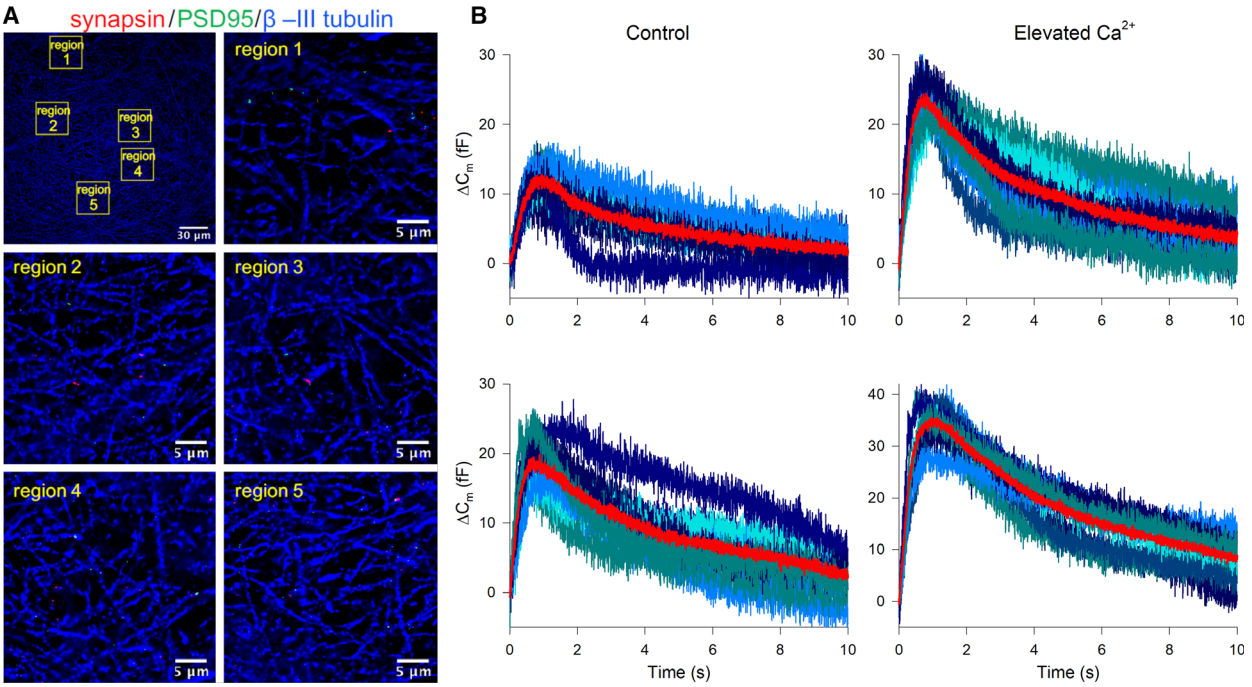

Fig. 3. hESC-derived DA neurons possess functioning presynaptic mechanism of vesicular neurotransmitter release. (A) Example image of coimmunostaining for PSD-95 (marker of postsynaptic densities) and synapsin (marker of presynaptic terminals) at DIV 77. Close proximity (≤ 1 μm) of PSD-95 (green) and synapsin (red) foci suggests availability of functional synapses in cell culture. Blue: staining for β-III tubulin, revealing cell somata and neurites. (B) Changes in whole-cell membrane capacitance evoked by stimulation series confirm elevated intensity of vesicle release. Shadows of blue: ten consequent individual traces; red: averaged trace. Elevated Ca^{2+} causes a significant increase in the area under the averaged curve (see text for statistics), thus confirming the involvement of presynaptic Ca^{2+}-dependent mechanisms. Top: 66 DIV culture; bottom: 100 DIV culture. Axis labels apply to all four plots.

obtained as 1.89 ± 0.15 for 66 DIV and 2.16 ± 0.1 for 100 DIV ($n = 7$ for both cases), with no significant difference between the two periods in culture: $P = 0.17$ for 66 DIV vs. 100 DIV, Student's *t*-test. This confirmed the functionality of the classical Ca^{2+}-dependent presynaptic vesicle release mechanism.

To further clarify synaptic functionality, we tried to record sPSCs generated by $GABA_A$Rs, AMPARs and NMDARs, under normal and elevated Ca^{2+} concentrations (Fig. 4). Our recordings revealed the presence of $GABA_A$R- and AMPAR-mediated sPSCs, which were suppressed by specific antagonists PTX and DNQX, respectively (Fig. 4A,B). Elevation of the extracellular Ca^{2+} concentration has caused a significant increase in sPSC frequency (Fig. 4C): 8.19 ± 1.14 Hz under control vs. 11.91 ± 1.39 Hz with elevated Ca^{2+}, $P = 0.029$ for $GABA_A$Rs 66 DIV; 11.85 ± 1.26 Hz vs. 18.87 ± 1.04 Hz, $P = 0.021$ for $GABA_A$Rs 100 DIV; 2.83 ± 0.49 Hz vs. 3.97 ± 0.57 Hz, $P = 0.0007$ for AMPARs 66 DIV; and 3.39 ± 0.39 Hz vs. 5.6 ± 0.55 Hz, $P = 0.023$ for AMPARs 100 DIV, $n = 6$ for all cases, Student's paired *t*-test. In this experiment, we observed a significant difference between sPSC frequency for $GABA_A$Rs at 66 and 100 DIV under elevated Ca^{2+} concentration: 11.91 ± 1.39 vs. 18.87 ± 1.04 Hz, respectively; $P = 0.0025$, $n = 12$, Student's *t*-test. In contrast, no spontaneous activity was observed when we isolated NMDARs pharmacologically (data not shown).

Therefore, we found that cultured DA neurons bear synapses with functional $GABA_A$Rs and AMPARs at the postsynaptic side and confirmed the release of both inhibitory (GABA) and excitatory (glutamate) neurotransmitters from the presynapse.

To explain the absence of NMDAR-generated postsynaptic response, we next hypothesized that, despite being abundant at the cell surface (Fig. 2A), NMDARs have too low rate of postsynaptic localization. To test this, we performed coimmunostaining of NR1 and NR2 NMDAR subunits and PSD-95 protein (Fig. 5A). We found that 0.75 ± 0.18% NMDAR-staining foci overlap with PSD-95 staining, and 0.85 ± 0.19% of PSD-95 staining foci overlap with NMDAR staining ($n = 10$ fields from three cultures). However, is this overlap rate low enough to prevent triggering of NMDAR-generated PSCs? To clarify

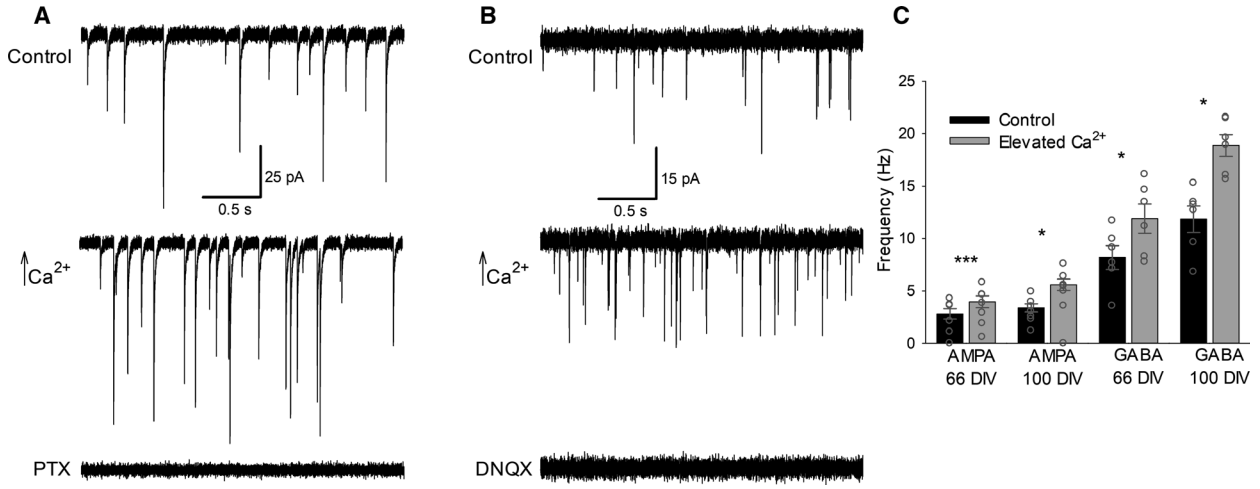

Fig. 4. Spontaneous activity confirms the presence of functional synapses in DA neurons. (A): $GABA_AR$-mediated sIPSCs. From top to bottom: control, elevated Ca^{2+}, PTX 50 μM. (B) AMPAR-mediated sEPSCs. From top to bottom: control, elevated Ca^{2+}, DNQX 20 μM. (C) Statistical summary for A and B: frequency of postsynaptic currents. Asterisks denote significance of difference between 'control' and 'elevated Ca^{2+}' conditions. $^*P < 0.05$, $^{***}P < 0.001$, $n = 6$, Student's paired *t*-test.

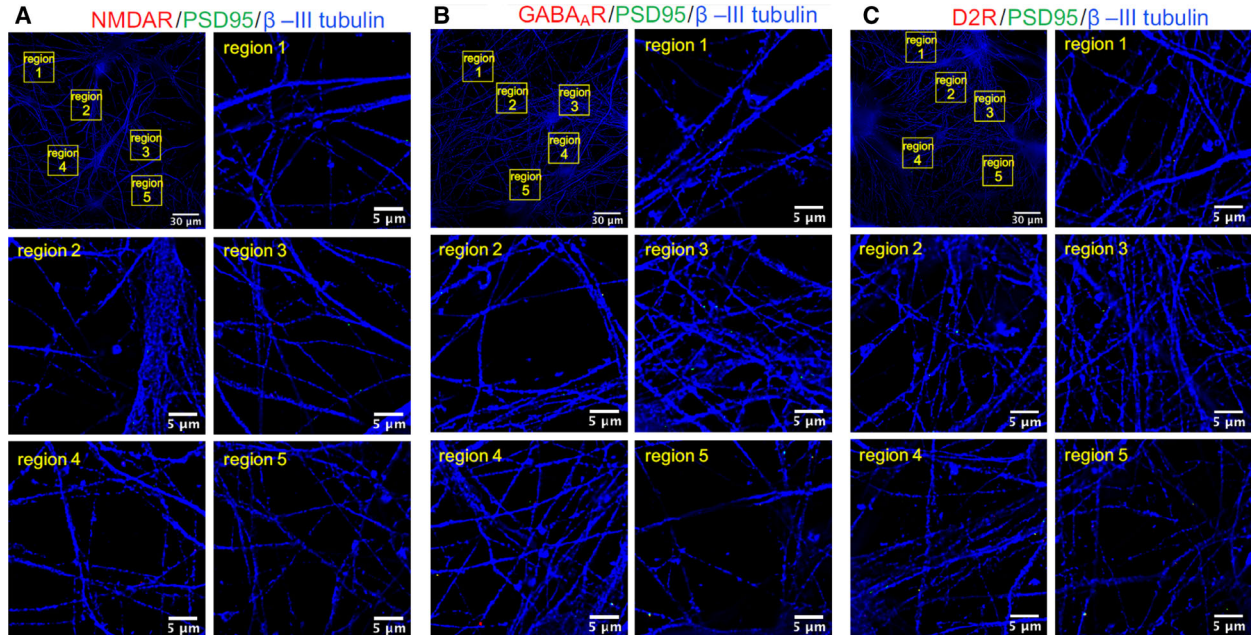

Fig. 5. Postsynaptic receptors in hESC-derived DA neurons. Example images of coimmunostaining for PSD-95 (marker of postsynaptic densities, green) and three receptors under study (red) in 77 DIV cultures – (A) NMDAR (staining for NR2A and NR2B subunits); (B) $GABA_AR$ (staining for α subunit); and (C) D2R. Blue: staining for β-III tubulin, revealing cell somata and neurites.

this, we performed coimmunostaining for the PSD-95 protein and α1 $GABA_AR$ subunit (Fig. 5B), since clear $GABA_AR$-mediated synaptic activity was registered in our previous experiment (Fig. 4A). Here, we found that $14.81 \pm 1.65\%$ $GABA_AR$-staining foci overlap with PSD-95 staining, and $13.04 \pm 1.04\%$ of PSD-95 staining foci overlap with $GABA_AR$ staining ($n = 8$ fields from two cultures). The difference between the overlap rates with PSD-95 for NMDAR and for $GABA_AR$ was highly significant: $P < 0.0001$ for both 'receptor over PSD-95' and 'PSD-95 over receptor' comparisons, Student's *t*-test.

However, even a single opening of NMDAR channel can be enough for proper transmission of synaptic signal [55]. Hence, relatively low (if compared to $GABA_A$Rs) level of NMDAR immunostaining would not cancel the ability of glutamatergic signals to evoke excitatory responses in postsynaptic cell; we thus decided to test the functional role of NMDARs with electrophysiological methods.

We assumed that there are the following possible mechanisms preventing normal NMDAR-mediated signalling.

First, activation of postsynaptic dopamine receptors of type 2 (D2R) by DA was shown to suppress NMDAR effects [50,56]. To substantiate this hypothesis, we performed coimmunostaining of D2R and PSD-95 (Fig. 5C) at 77 DIV. We found that 10.84 ± 3.13% of D2R staining foci overlap with PSD-95 staining, and 11.49 ± 3.38% of PSD-95 foci overlap with D2R staining (n = 7 fields from two cultures), thus giving credibility to this assumption.

Second, DA neurons may release an amount of DA high enough to block NMDARs directly [50,57]. To substantiate this hypothesis, we performed HPLC measurement of DA concentration in cell culture media. In this experiment, we detected a 1462.33 ± 365.58 nM (n = 2) of DA at 105 DIV, with no DA detection in control media (Fig. 6). With consideration of the native DA concentration in cerebrospinal fluid of 2–5 nM [58,59] and the brain extracellular volume fraction of ~ 0.2 [60], the results of the HPLC experiment suggest our hypothesis to be plausible.

Third, astroglial cells were shown to regulate the amount of NMDAR coagonists Gly and D-serine (D-Ser) directly by producing these compounds [61,62], or via the control over synthesis of substrate (such as L-serine) needed for production of the coagonists [63].

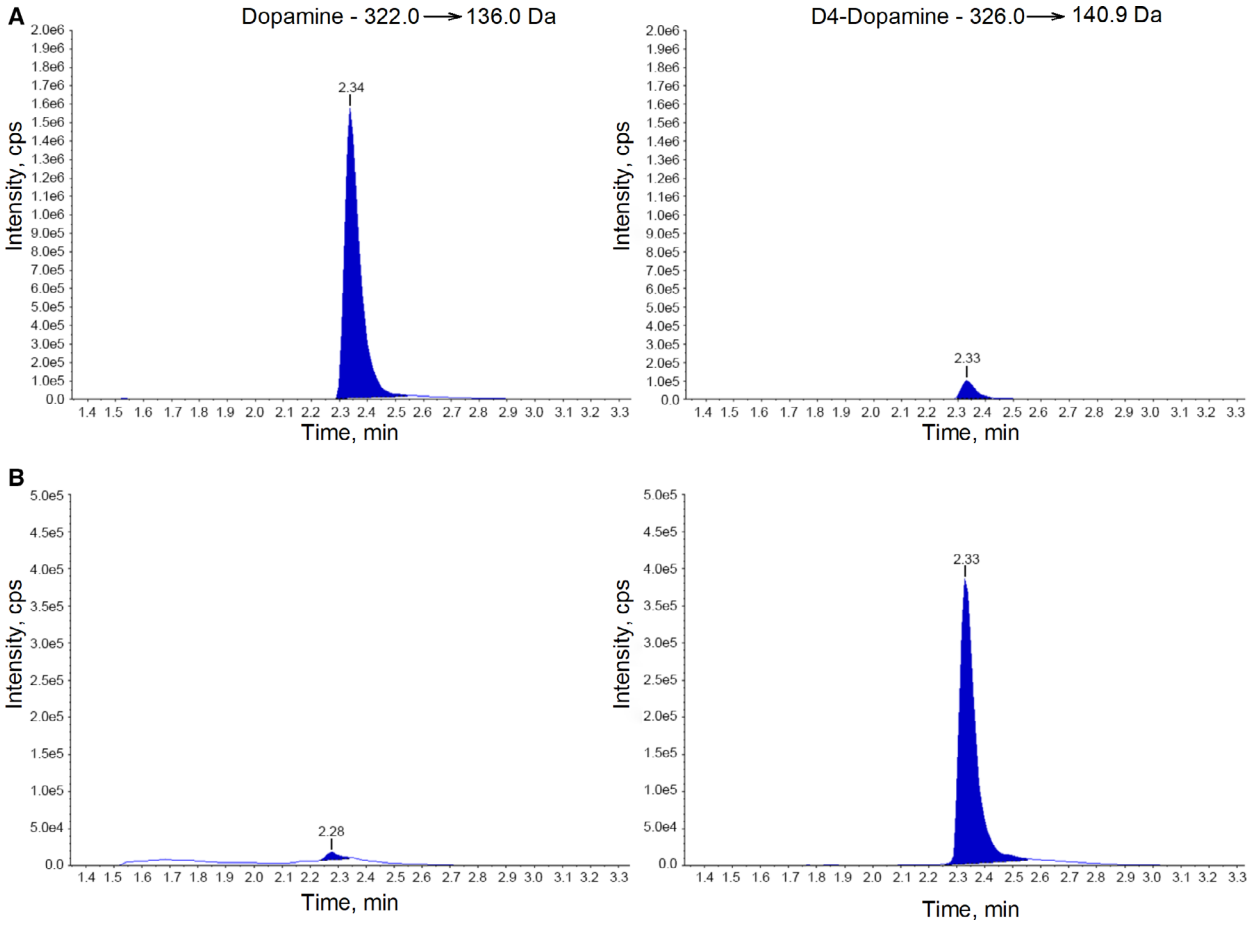

Fig. 6. Detection of DA in cell culture conditioned media by HPLC. (A) Conditioned media from 105 DIV cell culture. Dopamine quantification generated values of 224 ± 56 ng·mL^{-1}, or 1671 ± 587 ng/10^6 cells, or 1462 ± 365 nM·L^{-1}. (B) Control media. Right panels in A and B represent measurements of respective internal standard (1 ng of D4-dopamine).

Thus, the glia-free culture may not supply enough coagonists for proper NMDAR functioning.

To test these assumptions, we first attempted to record GlyR-mediated sPSCs in cultured neurons. However, neither 66 DIV (five recordings) nor 100 DIV (seven recordings) cells displayed visible postsynaptic events. But was this due to low Gly release in synapses, or due to the absence of GlyRs in cultured neurons? To clarify this, we performed an agonist-application experiment with nucleated patches. In this experiment, application of 100 μM Gly induced a clear inward current, fully suppressed by 1 μM strychnine (Fig. 7A). This suggested that the absence of glycinergic sPSCs was most likely due to a deficit of released Gly.

To test whether neuron-released DA causes a direct block of NMDARs, we repeated the rapid agonist-application experiment at nucleated patches, applying 100 μM NMDA + 100 μM Gly and 100 μM NMDA + 100 μM Gly + 500 μM DA (Fig. 7B). We found that DA decreases NMDAR response amplitude to 0.12 ± 0.03 of control: $P < 0.0001$ for the difference from unity, $n = 6$, Student's paired *t*-test.

Furthermore, we set out to comprehend whether under control conditions in our preparation NMDARs make a significant input into EPSC generation. To achieve this, we generated EPSPs with a series of five electrical stimuli 50 ms apart, using an experiment/control AUC ratio for quantification of the impact of pharmacological interventions (Fig. 7C). Fifty micro molar APV in this experiment did not exert a significant impact on AUC ratio: 0.95 ± 0.13 for DIV 66, $P = 0.75$ for the difference from unity; and 0.9 ± 0.11 for DIV 100, $P = 0.4$ for the difference from unity; $n = 6$ for both cases. There are two possible explanations for this result: first, due to the absence of functional NMDARs (but this is at odds with our previous data demonstrating NMDAR activity in patches; see Fig. 2A); and second, NMDARs under control conditions can be already suppressed due to the presence of an unknown factor.

Hence, to determine whether DA could be this suppressive factor, we tested whether DA receptors (DARs) of cultured neurons generate an inhibitory tone sufficient to suppress NMDAR signalling (Fig. 7D). The block of DARs' activity with 10 nM SCH 23390 (SCH) + 10 μM sulpiride (Sul) generated a discernible, but not significant, elevation of AUC above control values (Fig. 7D,K,L); AUC ratio for DIV 66: 1.37 ± 0.16, $P = 0.072$ for the difference from unity; $n = 6$, Student's paired *t*-test for this and all further AUC comparisons; and for DIV 100: 1.18 ± 0.099, $P = 0.135$ for the difference from unity. The 50 μM APV, added after SCH + Sul, decreased the AUC ratio to 1.26 ± 0.18 for DIV 66 and to 1.15 ± 0.15 for DIV 100; there was no significant difference in AUC under APV from SCH + Sul and from control: $P > 0.2$ for all comparisons.

Next, we examined whether suppression of NMDAR function can be overruled by additional amounts of NMDAR coagonists. First, we performed a 20-min incubation in 1 mM D-Isoleucine (D-Ile), since it was shown to stimulate release of Gly and D-Ser from primary neurons [64] (Fig. 7E,K,L). Incubation with D-Ile induced a significant increase in the AUC ratio: to 1.48 ± 0.1 for DIV 66, $P = 0.0047$ for the difference from unity; and to 1.42 ± 0.17 for DIV 100, $P = 0.048$ for the difference from unity. Application of APV returned AUC to control values: 0.88 ± 0.14 for DIV 66 and 1.07 ± 0.12 for DIV 100, $P > 0.4$ for the difference from unity for both cases. However, it is unclear whether incubation with D-Ile can reproduce the concentrations of NMDAR coagonists characteristic for neural tissue *in vivo*. Since native concentrations of Gly and D-Ser in *substantia nigra* – the brain area with abundant DA neurons – were found as 5.6 ± 1.3 μM (Gly) and 5.3 ± 1 μM (D-Ser) [65], we repeated the experiment adding 5 μM Gly + 5 μM D-Ser to the perfusion solution (Fig. 7F,K,L). We found that NMDAR coagonists increase the AUC ratio significantly: to 1.77 ± 0.15, $P = 0.004$ when compared to unity for DIV 66; and to 1.74 ± 0.19, $P = 0.011$ for DIV 100. Next, we tested whether the combined effects of DARs and Gly + D-Ser make a significant impact in our preparation. To do this, we blocked DARs with SCH + Sul after application of Gly + D-Ser (Fig. 7F,K,L). Inactivation of DARs did not cause a significant difference in AUC. The AUC ratio for Gly + D-Ser + SCH+Sul was obtained as 1.82 ± 0.17 for DIV 66 and 2.01 ± 0.13 for DIV 100, $P > 0.3$ in both cases when compared to correspondent values for Gly + D-Ser. Therefore, since antagonists of DA receptors (SCH and Sul) do not demonstrate a significant impact on NMDAR function when it was magnified by elevated concentrations of Gly + D-Ser, the possible effect of elevated DA concentration in cell culture medium is not transferred through DA receptors.

Finally, we assessed the direct effect of DA released upon field stimulation on postsynaptic NMDARs (Fig. 7G,K,L). To do this, we performed a 30-min incubation with 1 μM TBZ, which suppresses vesicle release of DA [66]. TBZ increased significantly the AUC ratio: to 1.3 ± 0.12, $P = 0.048$ when compared to unity for DIV 66, and to 1.26 ± 0.06, $P = 0.007$ for DIV 100. Further application of APV made the difference in AUC from control values nonsignificant: 0.89 ± 0.05 for DIV 66 and 0.96 ± 0.12 for DIV 100, $P > 0.08$ for both cases when compared to unity.

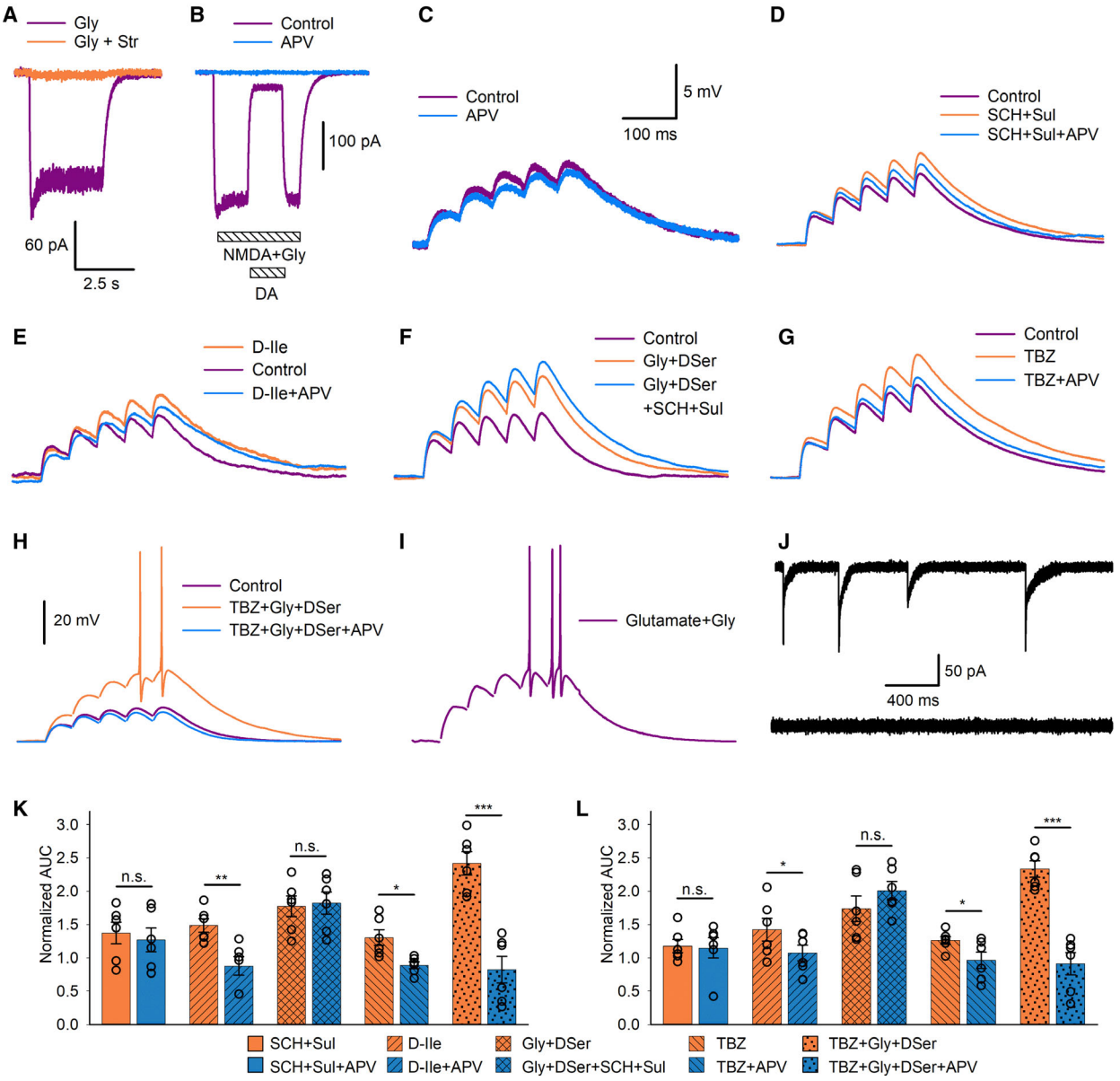

Fig. 7. NMDAR coagonists and DA modulate NMDAR signalling. (A) 100 μM Gly evoke inward current in nucleated patch, which is fully suppressed with 1 μM Str, thus confirming the presence of functional GlyRs in cultured neurons. 2.5-s scale bars apply to A and B. (B) 500 μM DA reversibly suppress NMDAR response generated in outside-out patch by application of 100 μM NMDA + 100 μM Gly. (C) Block of NMDARs with 50 μM APV does not make a significant impact on the area under the EPSP curve. 100-ms scale bars apply to C-I, 5-mV scale bars apply to C-G. In C-I stimulation, artefacts are blanked for clarity purpose. (D) Block of DARs with 10 nM SCH and 10 μM Sul induces nonsignificant increase in EPSP amplitude, which is then suppressed by APV. (E) 20-min incubation in 1 mM D-Ile induces an increase in EPSP amplitudes, which was reverted by APV. (F) 5 μM Gly + 5 μM D-Ser increase EPSP amplitudes, which are further increased by DARs block with SCH + Sul. (G) 20-min incubation in 1 μM TBZ induces an increase in EPSP amplitudes, which is reverted by APV. (H) 5 μM Gly + 5 μM D-Ser added to perfusion solution after 30-min. incubation in TBZ induces an increase in EPSP amplitudes and allows AP firing in response to field stimulation, whereas APV turns EPSP amplitudes back to control. 20-mV scale bars apply to H and I. (I) Series of rapid applications of Glu + Gly generate APs without a need to modify DAR signalling. (J) 5 μM Gly + 5 μM D-Ser and 30-min incubation in TBZ allow propagation of pharmacologically isolated NMDAR-mediated sPSCs (top trace), then fully suppressed by APV (bottom trace). (K) Statistical summary for D-H, 66 DIV cultures. Areas under the EPSP curve are normalized to those obtained under control conditions. Bar pattern legend apply to J and K. (L) Same as J, for 100 DIV cultures. Asterisks denote significance of difference between bars; $*P < 0.05$, $**P < 0.01$, $***P < 0.001$, n.s. – not significant, $n = 6$, Student's paired *t*-test.

Hence, we tested three possible factors that could silence NMDARs, and found that two of them – (a) lack of NMDAR coagonists and (b) direct suppression of NMDARs by synaptically released DA – made a significant impact on NMDAR function. However, no APs were observed in the experiments described above; that is, we still did not establish what prevents AP generation. We therefore decided to combine the effects of two significant factors. To do this, we repeated the experiment on EPSP AUC ratios with incubation in TBZ and application of Gly + D-Ser (Fig. 7H,K,L). The TBZ + Gly+ D-Ser caused a considerable increase in AUC; the AUC ratio was obtained as 2.42 ± 0.17 for 66 DIV, $P = 0.0005$ for the difference from unity, and as 2.33 ± 0.12, $P = 0.0001$ for 100 DIV. Further application of APV returned AUC to control values: 0.82 ± 0.2 and 0.91 ± 0.17 for 66 and 100 DIV, respectively, $P > 0.3$ for the difference from unity in both cases. And in this experiment, we observed AP generation in four cells out of six recorded for DIV 66 and in five out of six for DIV 100: see an example trace in Fig. 7H.

We therefore concluded that lack of NMDAR coagonists and a direct suppression of NMDAR function by DA released from neurons are the factors which, being combined, prevent neurons from firing. To confirm this, we conducted two control experiments.

First, we performed a series of rapid applications of 100 μM glutamate + 100 μM Gly at an isolated cell (connections to neighbouring neurons were cut with a blunt electrode); this should excite NMDARs without concomitant release of DA in synapses. In this experiment, four out of six recorded cells (DIV 66) and five out of eight cells (DIV 100) generated APs: refer to Fig. 7I for example trace. Second, we performed a whole-cell voltage-clamp recording after incubation with TBZ and adding Gly + D-Ser to the perfusion solution, with a ligand cocktail isolating NMDAR response. In this experiment, we set out to record NMDAR activation by spontaneous Glu release from presynaptic buttons. Such this type of NMDAR response (sPSCs) is difficult to obtain in any neuronal specimen, the probability of false-negative output was quite high. But, surprisingly, in three out of six cells (DIV 66) and five out of nine cells (DIV 100), we observed sPSCs; subsequent block of these sPSCs by APV confirmed their generation exclusively by NMDARs (Fig. 7J).

To further clarify the phenomenon of interneuronal crosstalk silencing in DA neuronal network, we studied the molecular mechanism of suppression of NMDAR activity by DA. At first, we tested whether DA blocks NMDAR functioning via the binding inside the ion channel. To do this, we recorded a current flow through NMDARs under nonsaturating concentrations of DA (200 μM) and NMDAR open-channel blocker memantine (Mem, 0.5 μM). In this experiment, an additive effect of DA and Mem (when they are applied together) implies independent action mechanisms; otherwise, these two compounds would compete for the same or nearby binding sites, that is DA likely binds inside the open NMDAR channel. Our data suggest the first scenario (Fig. 8A,B). Being applied separately at outside-out patches, DA and Mem suppressed the effect of 100 μM glutamate (Glu) + 100 μM Gly by $28.5 \pm 5.1\%$ and $42.1 \pm 6.9\%$, respectively, whereas their joint application reduced the NMDAR-transmitted current by $72.4 \pm 7.6\%$. The last value does not differ significantly from the sum of independent effects: $72.4 \pm 7.6\%$ vs. $70.6 \pm 7.8\%$, $P = 0.85$, $n = 7$, Student's t-test. The SE_{sum} value of 7.8% calculated with Eq. (4) for independent variables (see Materials and methods) appeared to be very close to that obtained in experiment for the joint application (7.6%), thus giving an additional support to our hypothesis about separate action sites of DA and Mem.

We therefore set out to test possible impact of DA on glutamate and glycine binding sites located at outer NMDAR surface. To do this, we analysed an NMDAR response decay kinetics due to dissociation of Gly and Glu. We performed a rapid solution application experiment on outside-out patches where the applied solution contained both Glu and Gly, whereas perfusion solution contained only one of these ligands. To test possible voltage dependence of DA effect, we repeated the experiment at −60 and +60 mV holding voltage (Fig. 8C,D). We found that 200 μM DA significantly augmented the fast-to-slow decay component ratio (DCR), that is accelerated the response decay of the current induced by the application of Gly but not Glu: see Fig. 8C legend for detailed description of calculation paradigm. The numerical output on DCR modulation was as follows: for Gly application at −60 mV 1.32 ± 0.23 under control vs. 2.35 ± 0.35 with DA, $P = 0.033$; at +60 mV 1.19 ± 0.1 vs. 1.91 ± 0.22, $P = 0.043$; for Glu application at −60 mV 1.15 ± 0.14 under control vs. 1.17 ± 0.15 with DA, $P = 0.86$; at +60 mV 1.2 ± 0.16 vs. 1.25 ± 0.15, $P = 0.67$; $n = 7$ for all comparisons, Student's paired t-test. This experimental result supports a hypothesis where the DA interaction is with the Gly binding site rather than the binding site of Glu.

To probe the hypothesis deeper, we performed an isobolic concentration–response analysis [67–69] of mixtures of DA with NMDAR antagonists with

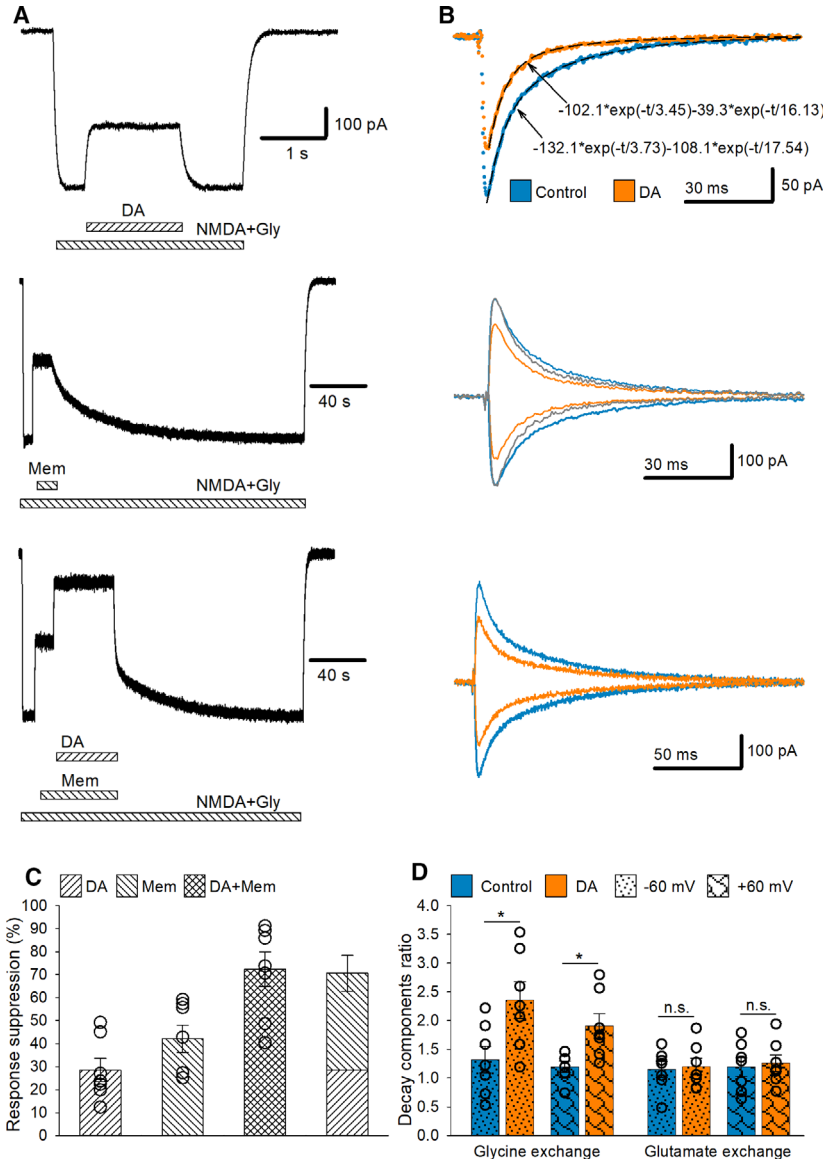

Fig. 8. Action mechanism of DA at NMDAR. (A) Example NMDAR-mediated currents recorded from the same nucleated patch, partially suppressed by DA (200 μM) and Mem (0.5 μM). 100-pA scale bars apply to all traces in A. (B) Statistical summary for A: percentage of control response suppression by DA and Mem. Height of the rightmost bar was obtained as a sum of DA and Mem effects when compounds were applied separately; SE value for this bar was calculated with Eq. (3) (see Materials and methods). (C) Top: analysis paradigm for NMDAR response decay kinetics with biexponential fitting. Dashed lines through data points: best-fit biexponential functions. Decay component ratio of fast (τ = 3.73) to slow (τ = 17.54) component generated by NMDAR ligands was obtained as 132.1/108.1 = 1.22; application of DA augmented the decay component ratio to 102.1/39.3 = 2.6. Colour codes for control and DA apply to all traces in C. Medium: rapid application of 100 μM glycine at −60 and +60 mV membrane potential, 100 μM glutamate added to both switching solutions. Grey: traces obtained under DA normalized to peak amplitude of control response to illustrate the impact of DA on decay kinetics. Bottom: rapid application of 100 μM glutamate at −60 and +60 mV membrane potential, 100 μM glycine added to both switching solutions. (D) Statistical summary of C. Asterisks denote significance of difference between bars: $*P < 0.05$, n.s. – not significant, Student's paired *t*-test.

different action mechanisms: Mem (open-channel blocker), PMPA (competitive antagonist of Glu binding site) and felbamate (Flb, competitive antagonist of Gly binding site). In this analysis paradigm, the concentration–effect curve of the drug mixture, which is significantly different (lower or higher) from a straight line connecting the effect values of pure components of the mixture, testifies to a nonadditive interaction (synergy or antagonism) of the components. This, in turn, suggests a common action site [67,70].

To perform the test under more physiological conditions, we evoked NMDAR response with native concentrations of the receptor's ligands characteristic for *substantia nigra*: 2.5 μM Glu + 5 μM Gly + 5 μM D-Ser [65]. However, with these concentrations of the agonists in experiment with rapid solution application (as at Fig. 2A) the NMDAR response amplitude and, as a sequence, signal-to-noise ratio were too small to generate a legible output upon application of antagonists, especially in their high concentrations. We therefore used a different experimental approach: continuous recording of single-channel NMDAR openings in outside-out patches with fluctuations of an OTF as a quantitative indicator of the antagonists' effect (Fig. 9).

At a first stage, we generated concentration–response curves for DA, Mem, Flb and PMPA and fitted them with a Hill equation, to obtain IC_{50} for

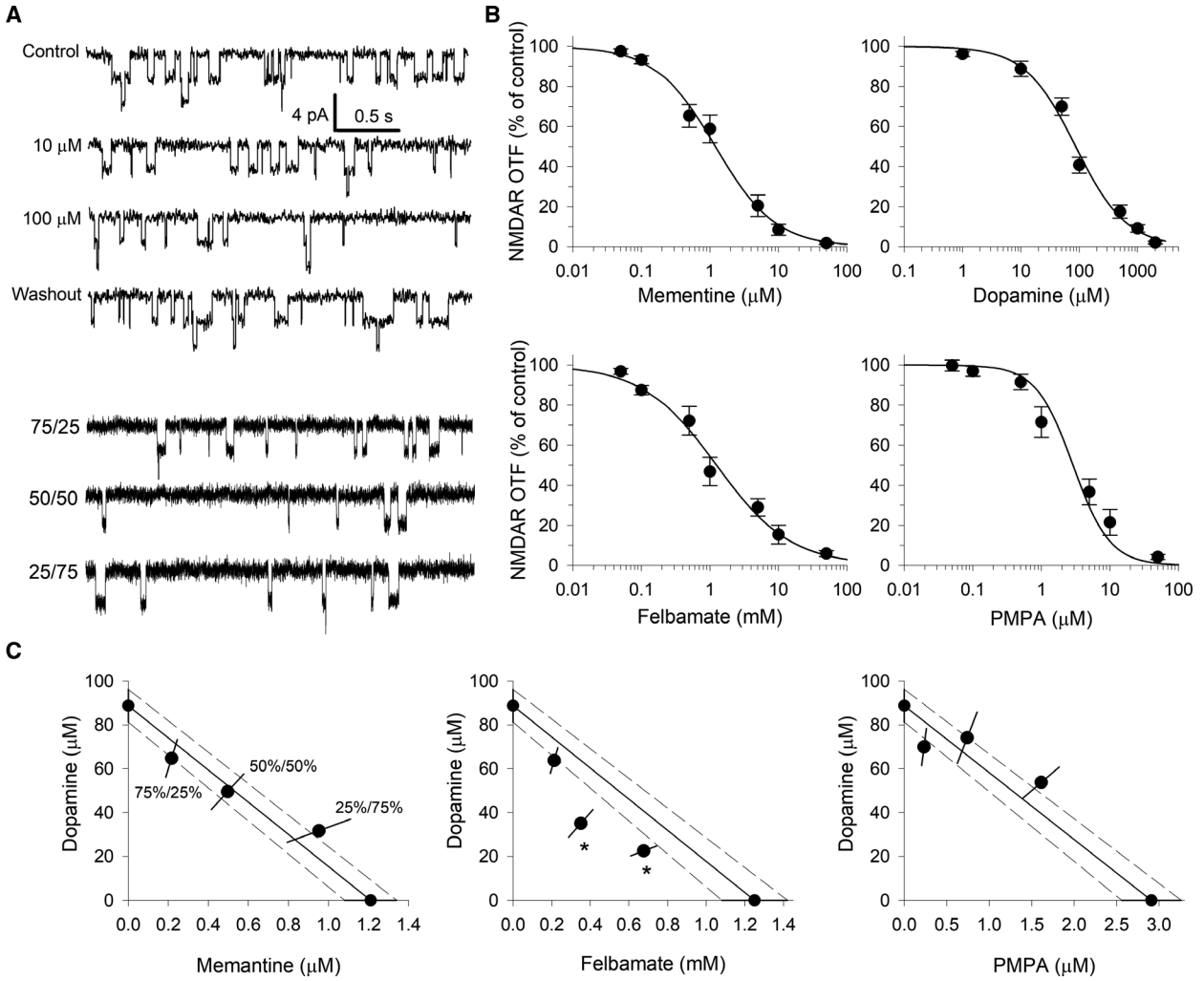

Fig. 9. Combined effects of NMDAR antagonists. (A) Example single-channel NMDAR recordings. Top four traces: effect of DA administered alone. From top to bottom: control, DA 10 μM, DA 100 μM, washout. Three bottom traces: effect of a mixture DA/ Flb in concentrations equal to their IC_{50}s. From top to bottom: 75% DA/ 25% Flb; 50% DA/ 50% Flb; 25% Da/ 75% Flb. Scale bars apply to all traces. (B) Dose–response curves for antagonists' impact on NMDAR OTF. Vertical axis labels apply to all panels. (C) Effect of combinations of IC_{50} for DA + Mem, DA + Flb and DA + PMPA. Dots on axes represent IC_{50} of DA (vertical axis) and other antagonist (horizontal axis) administered alone. The solid line connecting these dots represents the theoretical line of additivity for a continuum of different mixtures of antagonists' IC_{50}s. The dashed lines represent 95% confidentiality corridor for the corresponding solid line. In each plot, three dots between axes depict the experimentally obtained effect of IC_{50} mixtures of DA and other antagonist (see text for more details). From left to right, at each plot: 75% DA/ 25% of other antagonist, 50%/ 50%, 25% DA/ 75% of other antagonist. Position of each dot at a vector directed from the origin of coordinates to solid line represents a proportion of NMDAR OTF left intact after application of corresponding mixture. The IC_{50} mixture for DA-Flb pair (medium panel) displays a supra-additive interaction: dots depicting effects of 50%/ 50% and 25% DA/ 75% Flb ratios are significantly below the theoretical line of additivity (marked by asterisks, $P < 0.05$, Student's *t*-test, $n = 6$).

antagonists applied alone (Fig. 9B). The IC_{50} values were fitted out as follows: 88.76 ± 7.47 μM for DA, 1.21 ± 0.13 μM for Mem, 1.25 ± 0.17 mM for Flb and 2.91 ± 0.36 μM for PMPA. On top of that, the experiment with DA displayed a significant effect of 1 μM DA under native concentrations of NMDAR agonists: 96.19 ± 1.3% of NMDAR effect remained, $P = 0.033$ for the difference from 100%, $n = 6$, Student's paired *t*-test. This confirms a significant impact of DA concentration found in cell culture medium (1.4 μM, Fig. 6) on NMDAR functioning.

Next, we composed three mixtures of DA and other antagonists: 75% DA + 25% of an antagonist, 50% + 50% and 25% DA + 75% of an antagonist; all compounds were taken in concentrations equal to their IC_{50} values. The effect of these mixture was

compared with the theoretical line of additivity connecting IC_{50} values of the mixture components applied alone (Fig. 9C). Mixtures of 50% DA + 50% Flb and 25% DA + 75% Flb displayed a significant difference from half-maximum effect. For 50%/50% mixture, the remaining OTF was $33.77 \pm 6.05\%$ of control, $P = 0.043$ for the difference from half-maximum effect; for 25%/75% mixture, the remaining OTF was $39.4 \pm 3.93\%$ of control, $P = 0.047$ for the difference from half-maximum effect; $n = 6$ for both cases, paired Student's *t*-test. This result confirmed DA antagonist action at NMDAR to be associated with Gly binding site.

Discussion

In the current study, we used an established protocol that efficiently generates uniform DA neurons from hESCs expressing key developmental and biochemical markers [44,53,54]: see Fig. 2. Electrophysiological signature of our cultured neurons was also similar to DA neurons generated from hESCs by other groups and to that of native DA neurons. This signature includes the presence of functional NMDARs and AMPARs [27,71], $GABA_A$ receptors [36,72], GlyRs [37,73] and DA corelease with GABA [38] and glutamate [39]. We therefore concluded that neuronal cells differentiated in our study are biochemically and functionally similar to native DA neurons.

In this project, we revealed two main factors that prevent synaptic crosstalk in DA neural cultures when overlapping: lack of NMDAR coagonists and inhibition of NMDARs by synaptically released DA.

It is widely accepted that PSD-95 is a key element of postsynaptic density associated with postsynaptic NMDARs and $GABA_A$Rs [74,75]. Hence, a relatively high level of overlap between NMDAR and $GABA_A$R immune signal with that of PSD-95, observed in our study, is important evidence of morphologically developed synapses. Although the Dale's principle 'One neuron, one neurotransmitter' has been challenged decades ago, corelease of DA and glutamate was confirmed experimentally only quite recently [39,40]. From the two modes of glutamate-DA cotransmission evidenced so far: release from the different terminals or from the same terminal [76], our data suggest the presence of the latter mode, due to the significant impact of TBZ on the NMDAR effect in a continuously perfused recording chamber (Fig. 7G,H).

Physiological characterization of stem cell-derived DA neurons traditionally includes generation of APs by current injections in whole-cell current-clamp recording [77,78]. However, due to massive release of DA into the culture medium by DA neurons (Fig. 6) and significant impact of DA on NMDAR functioning (Fig. 7B), this approach may lead to biased characteristics of observed APs. Therefore, suppression of DA release and/or chelation of DA in extracellular solution is needed to reproduce a physiological environment for tested cells.

The concept of Gly and D-Ser as gliotransmitters, the concentration of which in cerebrospinal fluid is to a large extent regulated by astroglia, became popular during last two decades [79,80]. The concept gives rise to an obvious question as to what extent a given effect is generated by D-Ser and/or Gly released from primary neurons vs. astroglia, which triggers long-lasting emotional discussions [81,82]. Our experiments with D-Ile demonstrated that primary neurons alone cannot supply a sufficient amount of NMDAR coagonists for regular AP generation (Fig. 7D,J,K). This suggests astroglia to be if not a decisive, then, an important factor maintaining NMDAR signalling in DA neurons. Moreover, apart from release of coagonists into the extracellular space (studied in our work), regulatory impact of astroglia could potentially be translated through more indirect mechanisms, such as a 'serine shuttle' (regulation of L-serine/D-Ser balance) [63] or modulation of synthesis of tissue plasminogen activator [83], which, in turn, enhances NMDAR signalling [84]. On top of that, astroglia-released phosphatidic acid was shown to promote dendrite branching in cell culture, which enhances a number of NMDAR-containing glutamatergic synapses and NMDAR expression [85].

Direct interaction of DA receptors' ligands with NMDAR was repeatedly reported for at least several decades [50,57,86], but correspondent molecular action mechanisms still remain to a large extent unknown. Here, for the first time, we demonstrate that DA interacts with the Gly binding site, but neither acts as an open-channel blocker nor modulator of the Glu binding/dissociation. The lower effect of DA on positive membrane potential (Fig. 8C,D) may suggest a voltage-dependent nature of its action mechanism. Our observations are thus in line with an earlier report of voltage-dependent DA action at NMDAR, which was not changed under different Mg^{2+} concentrations [57]. However, such a complex nature of the DA effect manifestation prevents an immediate conclusion about its direct competitive interaction with Gly at NMDAR; rather, it may be a result of remote modulation of the Gly binding site.

The demand for neural grafts with minimum side effects has led to the application of a great deal of research efforts to find protocols that allow generation

of uniform neuronal populations from stem cells [87,88], in particular uniform populations of DA neurons [89]. However, proper neurogenesis and differentiation of neural cells require variable intercellular crosstalk with managing signals coming from neurons of different types [90,91] and from non-neuronal cells such as endothelial cells and astroglia [92,93]. This apparent discrepancy gives rise to a question as to what extent hESC-derived uniform neural cell preparations reproduce properties of target neurons developed in living tissue, in particular the pattern of interneuronal crosstalk and signal modulation in a neural network. To the best of our knowledge, until now there has been no evidence of AP generation in response to NMDAR-mediated interneuronal signalling in hESC-derived DA cultures, which questions the development of fundamental properties of neural networks such as synaptic strength and synaptic plasticity [94,95]. The absence of significant NMDAR input into AP generation observed in our first experiment on EPSPs (Fig. 2C) was in agreement with this situation. It is widely accepted that the number and strength of developing excitatory synapses are promoted by excitatory synaptic activity, in which NMDARs play a major role [85,96–98]. Hence, continuous silencing of NMDARs in DA neural culture may lead to synaptic underdevelopment and poor excitatory transmission. This, however, was not observed in our study: the experiment on AP generation displayed proper NMDAR-mediated transmission (Fig. 7G), although immunostaining revealed a significantly lower level of NMDAR–PSD-95 colocalization than that for $GABA_AR$–PSD-95 (Fig. 5). Furthermore, devoid of suppression by DA and supplied with native concentrations of Gly and D-Ser, excitatory synapses demonstrated adequate spontaneous NMDAR-mediated activity (Fig. 7I).

There are several possible explanations of these phenomena. First, silencing of synaptic NMDARs increases a number of excitatory synapses in the developing neural network [99]. Second, the intracellular C terminus of NMDAR was shown to be sufficient for proper synaptic formation and maturation independent of NMDAR ionotropic activity and gating [100]. Altogether, these factors may set a balance allowing normal synaptic development in pure DA neuronal cultures.

Acknowledgements

This work was supported by the Chancellor's Fellow Grant and the Moray Endowment Grant to SS. YC and TK were supported by Medical Research Council (Award Number: MR/K017276/1) and UK Centre for Mammalian Synthetic Biology. The authors gratefully acknowledge the financial support of NHS Research Scotland (NRS), through Edinburgh Clinical Research Facility. The authors thank Prof. Andrey Abramov (UCL) for his valuable suggestions on design of this study and Scott Denham from the Mass Spectrometry Core (Edinburgh) for his technical expertise and assistance in this work.

Author contributions

TK and SS conceived and supervised the study. TK provided tools and reagents. YC, SS, JS and NH performed experimental work. SS prepared the paper text. All authors contributed to experimental design and critically revised the paper text.

References

1 O'Rahilly RR and Müller F (2006) The Embryonic Human Brain: An Atlas of Developmental Stages. Chichester: John Wiley & Sons.
2 Reubinoff BE, Pera MF, Fong CY, Trounson A and Bongso A (2000) Embryonic stem cell lines from human blastocysts: somatic differentiation *in vitro*. *Nat Biotechnol* **18**, 399–404.
3 Thomson JA, Itskovitz-Eldor J, Shapiro SS, Waknitz MA, Swiergiel JJ, Marshall VS and Jones JM (1998) Embryonic stem cell lines derived from human blastocysts. *Science* **282**, 1145–1147.
4 Zhang SC, Wernig M, Duncan ID, Brustle O and Thomson JA (2001) *In vitro* differentiation of transplantable neural precursors from human embryonic stem cells. *Nat Biotechnol* **19**, 1129–1133.
5 Li XJ, Du ZW, Zarnowska ED, Pankratz M, Hansen LO, Pearce RA and Zhang SC (2005) Specification of motoneurons from human embryonic stem cells. *Nat Biotechnol* **23**, 215–221.
6 Perrier AL, Tabar V, Barberi T, Rubio ME, Bruses J, Topf N, Harrison NL and Studer L (2004) Derivation of midbrain dopamine neurons from human embryonic stem cells. *Proc Natl Acad Sci USA* **101**, 12543–12548.
7 Yan Y, Yang D, Zarnowska ED, Du Z, Werbel B, Valliere C, Pearce RA, Thomson JA and Zhang S-C (2005) Directed differentiation of dopaminergic neuronal subtypes from human embryonic stem cells. *Stem Cells* **23**, 781–790.
8 Zhang SC (2006) Neural subtype specification from embryonic stem cells. *Brain Pathol* **16**, 132–142.
9 Grace AA and Onn SP (1989) Morphology and electrophysiological properties of immunocytochemically identified rat dopamine neurons recorded *in vitro*. *J Neurosci* **9**, 3463–3481.
10 Stoker TB, Torsney KM and Barker RA (2018) Emerging treatment approaches for Parkinson's disease. *Front Neurosci* **12**, 693.

11 Muthuraman M, Koirala N, Ciolac D, Pintea B, Glaser M, Groppa S, Tamás G and Groppa S (2018) Deep brain stimulation and L-DOPA therapy: concepts of action and clinical applications in Parkinson's disease. *Front Neurol* **9**, 711.
12 Lindvall O, Sawle G, Widner H, Rothwell JC, Björklund A, Brooks D, Brundin P, Frackowiak R, Marsden CD, Odin P *et al.* (1994) Evidence for long-term survival and function of dopaminergic grafts in progressive Parkinson's disease. *Ann Neurol* **35**, 172–180.
13 Olanow CW, Goetz CG, Kordower JH, Stoessl AJ, Sossi V, Brin MF, Shannon KM, Nauert GM, Perl DP, Godbold J *et al.* (2003) A double-blind controlled trial of bilateral fetal nigral transplantation in Parkinson's disease. *Ann Neurol* **54**, 403–414.
14 Kefalopoulou Z, Politis M, Piccini P, Mencacci N, Bhatia K, Jahanshahi M, Widner H, Rehncrona S, Brundin P, Björklund A *et al.* (2014) Long-term clinical outcome of fetal cell transplantation for Parkinson disease: two case reports. *JAMA Neurol* **71**, 83–87.
15 Kikuchi T, Morizane A, Doi D, Magotani H, Onoe H, Hayashi T, Mizuma H, Takara S, Takahashi R, Inoue H *et al.* (2017) Human iPS cell-derived dopaminergic neurons function in a primate Parkinson's disease model. *Nature* **548**, 592–596.
16 Grealish S, Diguet E, Kirkeby A, Mattsson B, Heuer A, Bramoulle Y, Van Camp N, Perrier AL, Hantraye P, Björklund A *et al.* (2014) Human ESC-derived dopamine neurons show similar preclinical efficacy and potency to fetal neurons when grafted in a rat model of Parkinson's disease. *Cell Stem Cell* **15**, 653–665.
17 Schweitzer JS, Song B, Herrington TM, Park T-Y, Lee N, Ko S, Jeon J, Cha Y, Kim K, Li Q *et al.* (2020) Personalized iPSC-derived dopamine progenitor cells for Parkinson's disease. *N Engl J Med* **382**, 1926–1932.
18 Kirkeby A, Parmar M and Barker RA (2017) Strategies for bringing stem cell-derived dopamine neurons to the clinic: a European approach (STEM-PD). *Prog Brain Res* **230**, 165–190.
19 Studer L (2017) Strategies for bringing stem cell-derived dopamine neurons to the clinic-The NYSTEM trial. *Prog Brain Res* **230**, 191–212.
20 Brederlau A, Correia AS, Anisimov SV, Elmi M, Paul G, Roybon L, Morizane A, Bergquist F, Riebe I, Nannmark U *et al.* (2006) Transplantation of human embryonic stem cell-derived cells to a rat model of Parkinson's disease: effect of *in vitro* differentiation on graft survival and teratoma formation. *Stem Cells* **24**, 1433–1440.
21 Park C-H, Minn Y-K, Lee J-Y, Choi DH, Chang M-Y, Shim J-W, Ko J-Y, Koh H-C, Kang MJ, Kang JS *et al.* (2005) *In vitro* and *in vivo* analyses of human embryonic stem cell-derived dopamine neurons. *J Neurochem* **92**, 1265–1276.
22 Erceg S, Laínez S, Ronaghi M, Stojkovic P, Pérez-Aragó MA, Moreno-Manzano V, Moreno-Palanques R, Planells-Cases R and Stojkovic M (2008) Differentiation of human embryonic stem cells to regional specific neural precursors in chemically defined medium conditions. *PLoS One* **3**, e2122.
23 Francis KR and Wei L (2010) Human embryonic stem cell neural differentiation and enhanced cell survival promoted by hypoxic preconditioning. *Cell Death Dis* **1**, e22.
24 Steinbeck JA, Choi SJ, Mrejeru A, Ganat Y, Deisseroth K, Sulzer D, Mosharov EV and Studer L (2015) Optogenetics enables functional analysis of human embryonic stem cell–derived grafts in a Parkinson's disease model. *Nat Biotechnol* **33**, 204.
25 Erceg S, Ronaghi M, Zipancic I, Lainez S, Roselló MG, Xiong C, Moreno-Manzano V, Rodríguez-Jiménez FJ, Planells R, Alvarez-Dolado M *et al.* (2010) Efficient differentiation of human embryonic stem cells into functional cerebellar-like cells. *Stem Cells Dev* **19**, 1745–1756.
26 James OT, Livesey MR, Qiu J, Dando O, Bilican B, Haghi G, Rajan R, Burr K, Hardingham GE, Chandran S *et al.* (2014) Ionotropic GABA and glycine receptor subunit composition in human pluripotent stem cell-derived excitatory cortical neurones. *J Physiol* **592**, 4353–4363.
27 Malmersjö S, Liste I, Dyachok O, Tengholm A, Arenas E and Uhlén P (2010) Ca^{2+} and cAMP signaling in human embryonic stem cell-derived dopamine neurons. *Stem Cells Dev* **19**, 1355–1364.
28 Goparaju SK, Kohda K, Ibata K, Soma A, Nakatake Y, Akiyama T, Wakabayashi S, Matsushita M, Sakota M, Kimura H *et al.* (2017) Rapid differentiation of human pluripotent stem cells into functional neurons by mRNAs encoding transcription factors. *Sci Rep* **7**, 42367.
29 Schwirtlich M, Emri Z, Antal K, Máté Z, Katarova Z and Szabó G (2010) GABAA and GABAB receptors of distinct properties affect oppositely the proliferation of mouse embryonic stem cells through synergistic elevation of intracellular Ca2+. *FASEB J* **24**, 1218–1228.
30 Carpenter MK, Inokuma MS, Denham J, Mujtaba T, Chiu C-P and Rao MS (2001) Enrichment of neurons and neural precursors from human embryonic stem cells. *Exp Neurol* **172**, 383–397.
31 Cho MS, Lee Y-E, Kim JY, Chung S, Cho YH, Kim D-S, Kang S-M, Lee H, Kim M-H, Kim J-H *et al.* (2008) Highly efficient and large-scale generation of functional dopamine neurons from human embryonic stem cells. *Proc Natl Acad Sci USA* **105**, 3392–3397.

32 Johnson MA, Weick JP, Pearce RA and Zhang SC (2007) Functional neural development from human embryonic stem cells: accelerated synaptic activity via astrocyte coculture. *J Neurosci* **27**, 3069–3077.
33 Kim JE, O'Sullivan ML, Sanchez CA, Hwang M, Israel MA, Brennand K, Deerinck TJ, Goldstein LSB, Gage FH, Ellisman MH *et al.* (2011) Investigating synapse formation and function using human pluripotent stem cell-derived neurons. *Proc Natl Acad Sci USA* **108**, 3005–3010.
34 Kiiski H, Aanismaa R, Tenhunen J, Hagman S, Yla-Outinen L, Aho A, Yli-Hankala A, Bendel S, Skottman H and Narkilahti S (2013) Healthy human CSF promotes glial differentiation of hESC-derived neural cells while retaining spontaneous activity in existing neuronal networks. *Biol Open* **2**, 605–612.
35 Wu H, Pang ZP, Ge W, Kim KJ, Blanchi B, Chen C, Sudhof TC and Sun YE (2007) Integrative genomic and functional analyses reveal neuronal subtype differentiation bias in human embryonic stem cell lines. *Proc Natl Acad Sci USA* **104**, 13821–13826.
36 Parga JA, Rodriguez-Pallares J, Guerra MJ and Labandeira-Garcia JL (2007) Effects of GABA and GABA receptor inhibition on differentiation of mesencephalic precursors into dopaminergic neurons *in vitro*. *Dev Neurobiol* **67**, 1549–1559.
37 Wegner F, Kraft R, Busse K, Härtig W, Ahrens J, Leffler A, Dengler R and Schwarz J (2012) Differentiated human midbrain-derived neural progenitor cells express excitatory strychnine-sensitive glycine receptors containing $\alpha_2\beta$ subunits. *PLoS One* **7**, e36946.
38 Kim J-I, Ganesan S, Luo SX, Wu Y-W, Park E, Huang EJ, Chen L and Ding JB (2015) Aldehyde dehydrogenase 1a1 mediates a GABA synthesis pathway in midbrain dopaminergic neurons. *Science* **350**, 102–106.
39 Hnasko TS, Chuhma N, Zhang H, Goh GY, Sulzer D, Palmiter RD, Rayport S and Edwards RH (2010) Vesicular glutamate transport promotes dopamine storage and glutamate corelease *in vivo*. *Neuron* **65**, 643–656.
40 Stuber GD, Hnasko TS, Britt JP, Edwards RH and Bonci A (2010) Dopaminergic terminals in the nucleus accumbens but not the dorsal striatum corelease glutamate. *J Neurosci* **30**, 8229–8233.
41 Maximov A, Pang ZP, Tervo DG and Sudhof TC (2007) Monitoring synaptic transmission in primary neuronal cultures using local extracellular stimulation. *J Neurosci Methods* **161**, 75–87.
42 Kim JH, Auerbach JM, Rodríguez-Gómez JA, Velasco I, Gavin D, Lumelsky N, Lee S-H, Nguyen J, Sánchez-Pernaute R, Bankiewicz K (2002) Dopamine neurons derived from embryonic stem cells function in an animal model of Parkinson's disease. *Nature* **418**, 50–56.
43 Shi Y, Kirwan P, Smith J, Robinson HP and Livesey FJ (2012) Human cerebral cortex development from pluripotent stem cells to functional excitatory synapses. *Nat Neurosci* **15**, 477–486.
44 Chen Y, Dolt KS, Kriek M, Baker T, Downey P, Drummond NJ, Canham MA, Natalwala A, Rosser S and Kunath T (2019) Engineering synucleinopathy-resistant human dopaminergic neurons by CRISPR-mediated deletion of the SNCA gene. *Eur J Neurosci* **49**, 510–524.
45 Canham MA, Van Deusen A, Brison DR, De Sousa PA, Downie J, Devito L, Hewitt ZA, Ilic D, Kimber SJ, Moore HD *et al.* (2015) The molecular karyotype of 25 clinical-grade human embryonic stem cell lines. *Sci Rep* **5**, 17258.
46 Nolbrant S, Heuer A, Parmar M and Kirkeby A (2017) Generation of high-purity human ventral midbrain dopaminergic progenitors for *in vitro* maturation and intracerebral transplantation. *Nat Protoc* **12**, 1962–1979.
47 Zhang D, Wu L, Chow DS, Tam VH and Rios DR (2016) Quantitative determination of dopamine in human plasma by a highly sensitive LC-MS/MS assay: application in preterm neonates. *J Pharm Biomed Anal* **117**, 227–231.
48 O'Neill N and Sylantyev S (2019) Glutamate Receptor Probing with Rapid Application and Solution Exchange (RASE). *Methods Mol Biol* **1941**, 65–78.
49 Wang X, Zhong P, Gu Z and Yan Z (2003) Regulation of NMDA receptors by dopamine D4 signaling in prefrontal cortex. *J Neurosci* **23**, 9852–9861.
50 Kotecha SA, Oak JN, Jackson MF, Perez Y, Orser BA, Van Tol HH and MacDonald JF (2002) A D2 class dopamine receptor transactivates a receptor tyrosine kinase to inhibit NMDA receptor transmission. *Neuron* **35**, 1111–1122.
51 Beazely MA, Tong A, Wei W-L, Van Tol H, Sidhu B and MacDonald JF (2006) D2-class dopamine receptor inhibition of NMDA currents in prefrontal cortical neurons is platelet-derived growth factor receptor-dependent. *J Neurochem* **98**, 1657–1663.
52 Ku HH (1966) Notes on the use of propagation of error formulas. *J Res Natl Bur Stand* **70**, 263–273.
53 Andersson E, Tryggvason U, Deng Q, Friling S, Alekseenko Z, Robert B, Perlmann T and Ericson J (2006) Identification of intrinsic determinants of midbrain dopamine neurons. *Cell* **124**, 393–405.
54 Doi D, Samata B, Katsukawa M, Kikuchi T, Morizane A, Ono Y, Sekiguchi K, Nakagawa M, Parmar M and Takahashi J (2014) Isolation of human induced pluripotent stem cell-derived dopaminergic

progenitors by cell sorting for successful transplantation. *Stem Cell Rep* **2**, 337–350.
55 Nimchinsky EA, Yasuda R, Oertner TG and Svoboda K (2004) The number of glutamate receptors opened by synaptic stimulation in single hippocampal spines. *J Neurosci* **24**, 2054–2064.
56 Li Y-C, Xi D, Roman J, Huang Y-Q and Gao W-J (2009) Activation of glycogen synthase kinase-3β is required for hyperdopamine and D2 receptor-mediated inhibition of synaptic NMDA receptor function in the rat prefrontal cortex. *J Neurosci* **29**, 15551–15563.
57 Castro NG, de Mello MC, de Mello FG and Aracava Y (1999) Direct inhibition of the N-methyl-D-aspartate receptor channel by dopamine and (+)-SKF38393. *Br J Pharmacol* **126**, 1847–1855.
58 Perry KW and Fuller RW (1992) Effect of fluoxetine on serotonin and dopamine concentration in microdialysis fluid from rat striatum. *Life Sci* **50**, 1683–1690.
59 Baker AJ, Zornow MH, Scheller MS, Yaksh TL, Skilling SR, Smullin DH, Larson AA and Kuczenski R (1991) Changes in extracellular concentrations of glutamate, aspartate, glycine, dopamine, serotonin, and dopamine metabolites after transient global ischemia in the rabbit brain. *J Neurochem* **57**, 1370–1379.
60 Madelin G, Kline R, Walvick R and Regatte RR (2014) A method for estimating intracellular sodium concentration and extracellular volume fraction in brain *in vivo* using sodium magnetic resonance imaging. *Sci Rep* **4**, 4763.
61 Schell MJ, Molliver ME and Snyder SH (1995) D-serine, an endogenous synaptic modulator: localization to astrocytes and glutamate-stimulated release. *Proc Natl Acad Sci USA* **92**, 3948–3952.
62 Harsing LG and Matyus P (2013) Mechanisms of glycine release, which build up synaptic and extrasynaptic glycine levels: the role of synaptic and non-synaptic glycine transporters. *Brain Res Bullet* **93**, 110–119.
63 Neame S, Safory H, Radzishevsky I, Touitou A, Marchesani F, Marchetti M, Kellner S, Berlin S, Foltyn VN, Engelender S *et al.* (2019) The NMDA receptor activation by d-serine and glycine is controlled by an astrocytic Phgdh-dependent serine shuttle. *Proc Natl Acad Sci USA* **116**, 20736–20742.
64 Rosenberg D, Artoul S, Segal AC, Kolodney G, Radzishevsky I, Dikopoltsev E, Foltyn VN, Inoue R, Mori H, Billard J-M *et al.* (2013) Neuronal D-serine and glycine release via the Asc-1 transporter regulates NMDA receptor-dependent synaptic activity. *J Neurosci* **33**, 3533–3544.
65 Tossman U, Jonsson G and Understedt U (1986) Regional distribution and extracellular levels of amino acids in rat central nervous system. *Acta Physiol Scand* **127**, 533–545.
66 Hayden MR, Leavitt BR, Yasothan U and Kirkpatrick P (2009) Tetrabenazine. *Nat Rev Drug Discov* **8**, 17–18.
67 Murado García MA and Prieto Lage M (2013) Dose-response analysis in the joint action of two effectors. A new approach to simulation, identification and modelling of some basic interactions. *PLoS One* **8**, e61391.
68 Sylantyev S and Zinkovsky V (2002) Optimization of a mixture of an agonist and an antagonist of the GABA-receptor system according to the safety criterion. *Neurophysiology* **34**, 243–246.
69 Oloś G, Zinkovsky VG, Zhuk M and Zhuk OV (2010) A molecular model and a method of isodynamic analysis of combined effects of constant xenobiotic concentrations. In Proceeding of the XVI National Conference on Applications of Mathematics in Biology and Medicine, pp. 82–87. AGH University of Science and Technology, Kraków.
70 Luszczki JJ, Wojcik-Cwikla J, Andres MM and Czuczwar SJ (2005) Pharmacological and behavioral characteristics of interactions between vigabatrin and conventional antiepileptic drugs in pentylenetetrazole-induced seizures in mice: an isobolographic analysis. *Neuropsychopharmacology* **30**, 958–973.
71 Blythe SN, Atherton JF and Bevan MD (2007) Synaptic activation of dendritic AMPA and NMDA receptors generates transient high-frequency firing in substantia nigra dopamine neurons *in vitro*. *J Neurophysiol* **97**, 2837–2850.
72 Tepper JM and Lee CR (2007) GABAergic control of substantia nigra dopaminergic neurons. In Progress in Brain Research (Tepper JM, Abercrombie ED and Bolam JP eds), pp. 189–208. Elsevier, Amsterdam.
73 Zheng F and Johnson SW (2001) Glycine receptor-mediated inhibition of dopamine and non-dopamine neurons of the rat ventral tegmental area *in vitro*. *Brain Res* **919**, 313–317.
74 Kornau H, Schenker L, Kennedy M and Seeburg P (1995) Domain interaction between NMDA receptor subunits and the postsynaptic density protein PSD-95. *Science* **269**, 1737–1740.
75 Fritschy J-M, Schweizer C, Brünig I and Lüscher B (2003) Pre- and post-synaptic mechanisms regulating the clustering of type A γ-aminobutyric acid receptors (GABAA receptors). *Biochem Soc Trans* **31**, 889–892.
76 Broussard JI (2012) Co-transmission of dopamine and glutamate. *The J Gen Physiol* **139**, 93–96.
77 Paşca SP, Portmann T, Voineagu I, Yazawa M, Shcheglovitov A, Paşca AM, Cord B, Palmer TD, Chikahisa S, Nishino S *et al.* (2011) Using iPSC-derived neurons to uncover cellular phenotypes associated with Timothy syndrome. *Nat Med* **17**, 1657–1662.

78 Hartfield EM, Yamasaki-Mann M, Ribeiro Fernandes HJ, Vowles J, James WS, Cowley SA and Wade-Martins R (2014) Physiological characterisation of human iPS-derived dopaminergic neurons. *PLoS One* **9**, e87388.
79 Halassa MM, Fellin T and Haydon PG (2007) The tripartite synapse: roles for gliotransmission in health and disease. *Trends Mol Med* **13**, 54–63.
80 Petrelli F and Bezzi P (2016) Novel insights into gliotransmitters. *Curr Opin Pharmacol* **26**, 138–145.
81 Papouin T, Henneberger C, Rusakov DA and Oliet SHR (2017) Astroglial versus Neuronal D-Serine: fact checking. *Trends Neurosci* **40**, 517–520.
82 Wolosker H, Balu DT and Coyle JT (2017) Astroglial versus neuronal d-serine: check your controls! *Trends Neurosci* **40**, 520–522.
83 Tran ND, Schreiber SS and Fisher M (1998) Astrocyte regulation of endothelial tissue plasminogen activator in a blood-brain barrier model. *J Cerebral Blood Flow Metab* **18**, 1316–1324.
84 Nicole O, Docagne F, Ali C, Margaill I, Carmeliet P, MacKenzie ET, Vivien D and Buisson A (2001) The proteolytic activity of tissue-plasminogen activator enhances NMDA receptor-mediated signaling. *Nat Medi* **7**, 59–64.
85 Zhu Y-B, Gao W, Zhang Y, Jia F, Zhang H-L, Liu Y-Z, Sun X-F, Yin Y and Yin D-M (2016) Astrocyte-derived phosphatidic acid promotes dendritic branching. *Sci Rep* **6**, 21096.
86 Gandolfi O and Dall'Olio R (1996) Modulatory role of dopamine on excitatory amino acid receptors. *Prog Neuropsychopharmacol Biol Psychiatry* **20**, 659–671.
87 Bibel M, Richter J, Lacroix E and Barde YA (2007) Generation of a defined and uniform population of CNS progenitors and neurons from mouse embryonic stem cells. *Nat Protoc* **2**, 1034–1043.
88 Ladewig J, Koch P, Endl E, Meiners B, Opitz T, Couillard-Despres S, Aigner L and Brustle O (2008) Lineage selection of functional and cryopreservable human embryonic stem cell-derived neurons. *Stem Cells* **26**, 1705–1712.
89 Chambers SM, Fasano CA, Papapetrou EP, Tomishima M, Sadelain M and Studer L (2009) Highly efficient neural conversion of human ES and iPS cells by dual inhibition of SMAD signaling. *Nat Biotechnol* **27**, 275.
90 Ohnuma S-I and Harris WA (2003) Neurogenesis and the cell cycle. *Neuron* **40**, 199–208.
91 Deng W, Aimone JB and Gage FH (2010) New neurons and new memories: how does adult hippocampal neurogenesis affect learning and memory? *Nat Rev Neurosci* **11**, 339.
92 Ninkovic J and Götz M (2007) Signaling in adult neurogenesis: from stem cell niche to neuronal networks. *Curr Opin Neurobiol* **17**, 338–344.
93 Lledo P-M, Alonso M and Grubb MS (2006) Adult neurogenesis and functional plasticity in neuronal circuits. *Nat Rev Neurosci* **7**, 179–193.
94 Calabresi P, Picconi B, Tozzi A and Di Filippo M (2007) Dopamine-mediated regulation of corticostriatal synaptic plasticity. *Trends Neurosci* **30**, 211–219.
95 Zweifel LS, Argilli E, Bonci A and Palmiter RD (2008) Role of NMDA receptors in dopamine neurons for plasticity and addictive behaviors. *Neuron* **59**, 486–496.
96 Burrone J, O'Byrne M and Murthy VN (2002) Multiple forms of synaptic plasticity triggered by selective suppression of activity in individual neurons. *Nature* **420**, 414–418.
97 Turrigiano GG, Leslie KR, Desai NS, Rutherford LC and Nelson SB (1998) Activity-dependent scaling of quantal amplitude in neocortical neurons. *Nature* **391**, 892–896.
98 Zhang LI and Poo M-M (2001) Electrical activity and development of neural circuits. *Nat Neurosci* **4**, 1207–1214.
99 Adesnik H, Li G, During MJ, Pleasure SJ and Nicoll RA (2008) NMDA receptors inhibit synapse unsilencing during brain development. *Proc Natl Acad Sci USA* **105**, 5597–5602.
100 Gambrill AC and Barria A (2011) NMDA receptor subunit composition controls synaptogenesis and synapse stabilization. *Proc Natl Acad Sci USA* **108**, 5855–5860.